

ION ROCKET SYSTEM RESEARCH AND DEVELOPMENT

by

G. C. Reid, F. A. Barcatta, G. Sohl, and R. C. Speiser

prepared for

NATIONAL AERONAUTICS AND SPACE ADMINISTRATION

CONTRACT NAS3-5250

OTS PRICE

XEROX

MICROFILM

\$

\$

FACILITY FORM 502

N64-29495
(ACCESSION NUMBER)
123
(PAGES)
CR-54026
(NASA CR OR TMX OR AD NUMBER)

(THRU)

(CODE)

(CATEGORY)

EOS

ELECTRO-OPTICAL SYSTEMS, INC., PASADENA, CALIFORNIA

CASE FILE COPY

NOTICE

This report was prepared as an account of Government sponsored work. Neither the United States, nor the National Aeronautics and Space Administration (NASA), nor any person acting on behalf of NASA:

- A.) Makes any warranty or representation, expressed or implied, with respect to the accuracy, completeness, or usefulness of the information contained in this report, or that the use of any information, apparatus, method, or process disclosed in this report may not infringe privately owned rights; or
- B.) Assumes any liabilities with respect to the use of, or for damages resulting from the use of any information, apparatus, method or process disclosed in this report.

As used above, "person acting on behalf of NASA" includes any employee or contractor of NASA, or employee of such contractor, to the extent that such employee or contractor of NASA, or employee of such contractor prepares, disseminates, or provides access to, any information pursuant to his employment or contract with NASA, or his employment with such contractor.

Requests for copies of this report should be referred to

National Aeronautics and Space Administration
Office of Scientific and Technical Information
Attention: AFSS-A
Washington, D.C. 20546

1183

QUARTERLY REPORT

ION ROCKET SYSTEM RESEARCH AND DEVELOPMENT

by

G. C. Reid, F. A. Barcatta, G. Sohl, and R. C. Speiser

prepared for

NATIONAL AERONAUTICS AND SPACE ADMINISTRATION

20 September 1964

CONTRACT NAS3-5250

Technical Management
NASA Lewis Research Center
Cleveland, Ohio
Spacecraft Technology Division
James Wolters

ELECTRO-OPTICAL SYSTEMS, INC.

300 No. Halstead Street
Pasadena, California

ABSTRACT

2 9495'

Work performed in the second quarter of a research and development program on an electron bombardment cesium ion rocket system is reported. A long duration engine system test is described including operating parameters during the run and analyses of components upon termination of the test. A new permanent magnet engine is reported and the results of plasma distribution studies and autocathode tests are discussed.

auth.

TABLE OF CONTENTS

	<u>Page</u>
1. INTRODUCTION	1
1.1 Program Objectives	1
1.2 Status of Beginning of Quarter	1
1.3 General Status	2
1.4 Key Personnel	2
2. ELECTRODE TESTS	3
2.1 High Drain Current Condition	3
2.2 Heated Molybdenum Electrode Test	6
2.3 Cooled Copper Electrode Tests	9
3. LONG DURATION TEST	11
3.1 Operating Conditions and Time History	11
3.2 Residual Drains	16
3.3 Condition of Engine After Test	19
4. FEED SYSTEM	30
4.1 Analysis of Feed System After Test	30
4.2 Feed System Improvements	35
5. PERMANENT MAGNET STUDIES	39
5.1 Permanent Magnet Engine Design	39
5.2 Permanent Magnet Engine Test	42
6. PLASMA DISTRIBUTION STUDIES	42
6.1 Ion Efflux Distributions	42
6.2 LN ₂ Cooled Neutral Detector	49
7. AUTOCATHODE IMPROVEMENT STUDIES	49
7.1 Autocathode Tests	52
7.2 Cathode Starting Power	52
8. QUALITY ASSURANCE	54
9. PLANS FOR NEXT QUARTER	54

ILLUSTRATIONS

	<u>Page</u>
1. Residual drain current versus gap voltage	4
2. Residual drain current versus gap voltage for two polarities	4
3. Temperature and oxygen dependence of drain current	7
4. Cathode mounting plate after high drain test	7
5. Cooled copper accelerator electrode	10
6. Vaporizer power history for 281 hour test	12
7. Drain current versus time for 201 hour test	12
8. Accelerating electrode temperature and drain current after test termination	17
9. Accelerator drain current versus gap voltage	17
10. Drain current versus gap voltage for reversed polarity test	18
11. Schottky plot for reversed voltage test	18
12. DER-1 engine system after 281 hour test	20
13. Cathode and orifice plate	21
14. Anode and chamber interior	21
15. Engine shell	22
16. Insulators	24
17. Screen electrode	24
18. Accelerating electrode - downstream side	25
19. Cross section of deep pit	25
20. Cross section of shallow pit	26
21. Accelerating electrode - upstream side	26
22. Feed system components	31
23. End view of vaporizer surface	31
24. Porous rod and vaporizer assembly	32

ILLUSTRATIONS (cont.)

		<u>Page</u>
25.	Location of samples taken for analysis	32
26.	Manually operated cesium valve	38
27.	Manual valve	38
28.	750-hour feed system	40
29.	Permanent magnet engine design	41
30.	Permanent magnet engine	43
31.	Ion beam current density distributions	45
32.	Variation of ion current density distribution with source potential	47
33.	Variation of ion current density distribution with Accelerator potential	48
34.	Variation of ion current density distribution with magnetic field	50
35.	Liquid nitrogen cooled, scanning neutral detector	51

LIST OF TABLES

I	Engine Operating Parameters During 201 Hour Continuous Test	14
II	Analyses of Deposits on Components	28
III	Component Weight Changes	29
IV	Analysis of Porous Rod	33
V	Analysis of Cesium Samples	34
VI	Weights and Dimensions of Feed System Components	36
VII	DE and Permanent Magnet Engine Weights	44
VIII	Source Efficiency with External Heater Cathodes	53

SUMMARY

This quarterly report for the period 1 June 1964 to 31 August 1964 describes the work performed under Contract NAS3-5250. The objectives of the program are to continue the development and testing of the engine and feed system developed under Contract NAS3-2516; to investigate the use of permanent magnets with the electron bombardment cesium ion engine; to study the plasma distribution in electron bombardment cesium ion sources; and to make improvements in the cesiated autocathodes used in the engines.

During the period electrode drain currents due to electron emission from a low work function composite surface (Cs-O-Mo) were encountered and investigated. An engine and zero-g feed system were tested for 281 hours, the last 201 hours of which were continuous. After the test, which was terminated voluntarily, engine and feed system components were thoroughly analyzed and contamination of surfaces and component weight changes were found to be small. The erosion of the accelerating electrode (which was made of copper) indicated an extrapolated lifetime of a few thousand hours.

A permanent magnet engine, in which the shell is the magnet, was designed and fabricated. This engine weighs about 60% as much as the electromagnet design which underwent the long test. Initial tests of the permanent magnet engine were performed.

Ion beam current density distributions were obtained for a wide variety of operating parameters. In general, the distribution tends to be more uniform for lower magnetic field intensities and for higher accelerating potentials. Several autocathode designs were fabricated and tested and the technique of heating the autocathode (for engine start-up) using the arc power supply was investigated and found to be feasible.

1. INTRODUCTION

This is the second Quarterly Report under Contract NAS3-5250, ION ROCKET SYSTEM RESEARCH AND DEVELOPMENT. Throughout the text, reference will be made to the first Quarterly Report of the program, NASA CR-54025 (EOS Report 4920-Q-1), which is available through the NASA Office of Scientific and Technical Information.

1.1 Program Objectives

The present program provides for the continued development and testing of the DE engine and feed system to achieve demonstrated long life and reliability. It includes the elimination of short and long term failure modes and the evaluation of lifetime limitations. A quality assurance and reliability program is being followed on this task.

In addition to the long-life engine and feed system program, three research and development programs are being pursued. They are:

1. Design, fabrication, and testing of a permanent magnet version of the DE engine.
2. Plasma distribution studies to investigate basic means of improving engine operation and lifetime.
3. Autocathode improvement studies to reduce the starting power requirements of cesium electron bombardment ion engines.

1.2 Status of Beginning of Quarter

During the last quarter, a test facility for lifetime and reliability testing of the DE engine and feed system had been prepared and initial testing begun. A permanent magnet modification of the DE engine was fabricated and operated and its performance was comparable to that of the electromagnet engine.

Plasma distribution studies were undertaken and ion and neutral efflux distributions from a bombardment engine were determined. The effects of the magnetic field intensity and cathode orifice configuration on the ion and neutral efflux distributions were investigated. The performance of the DE engine using different cathode orifice sizes had been investigated and minimum autocathode starting temperatures were determined. Start-ups had been made without using the internal cathode heater and an autocathode configuration with no internal heater had been designed, fabricated, and tested.

1.3 General Status

During the second quarter, a high electrode drain current condition was encountered and investigated. A DE engine system with a copper accelerating electrode was operated for 281 hours, the last 201 hours of which were continuous. The engine and zero-g feed system were thoroughly analyzed after the test.

A new permanent magnet engine, in which the engine shell is the magnet, was designed and fabricated and testing of the engine was begun. Ion efflux distributions for a wide variety of parameters were obtained with the scanning Faraday probe. A liquid nitrogen cooled neutral cesium detector for scanning the neutral efflux within the ion beam was designed and fabricated.

Several externally heated autocathode designs were fabricated and tested and the feasibility of heating the autocathode (for start-up) using the arc power supply was investigated.

1.4 Key Personnel

The key personnel on the program, and their areas of effort are:

R. C. Speiser	Program Supervisor
G. C. Reid	Long Life Engine
F. A. Barcatta	Long Life Feed System
G. Sohl	Applied Research
S. Zafran	Quality Assurance

These personnel supervise their respective tasks and are the major contributors to the program and to all reports generated under the program.

2. ELECTRODE TESTS

At the end of the first quarter (EOS Report 4920-Q-1; NASA CR-54025), a run was terminated after 23 hours operation due to high drain currents (>25 ma). These high drain conditions, encountered with a molybdenum accelerating electrode, were further investigated.

2.1 High Drain Current Condition

After the 23 hour test was terminated, high voltage was turned back on and the drains were measured as a function of accelerator gap voltage as the engine cooled. The results are shown in Figure 1. The temperatures were measured at the engine shell and are only roughly indicative of the screen electrode or accelerator electrode temperatures. The drain current - gap voltage relationship is highly non-linear and suggests a field enhanced emission effect although the temperatures and the magnitude of the field in the gap are much too low to give these phenomena for cesiated molybdenum.

After a long cooling period, the engine was restarted and after several hours high drains were again encountered. The feed system and arc power were removed and the data of Figure 2 were taken. For the two sets of data taken for normal polarity, the differences in the data are partly due to cooling of the system but there does appear to be a significant hysteresis effect. The voltages applied to the electrodes were then reversed and the third set of data was taken. The higher current for this case is significant as it indicates that the electrode surface effect giving rise to the drain current is more pronounced on the screen electrode than on the accelerating electrode. Since the screen electrode runs hotter and presumably stays hotter than the accelerating electrode during the time both are cooling, the higher current with reversed polarity is consistent with an electron emission hypothesis.

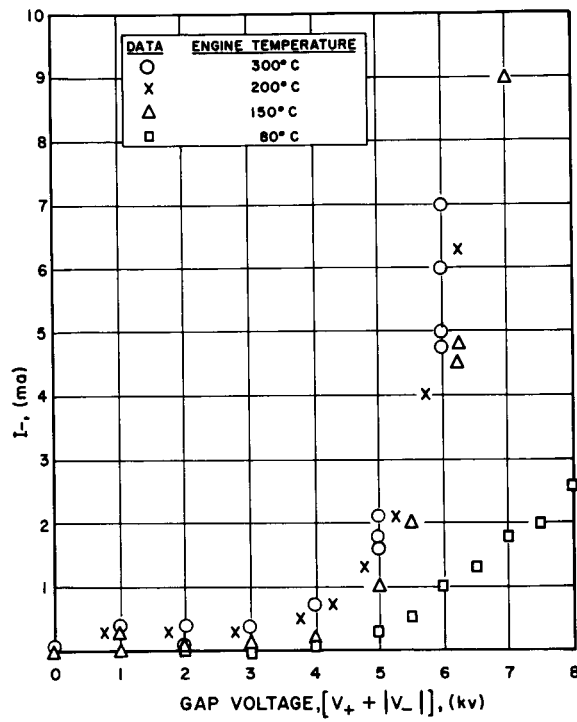


FIG. 1
RESIDUAL DRAIN CURRENT
VS GAP VOLTAGE

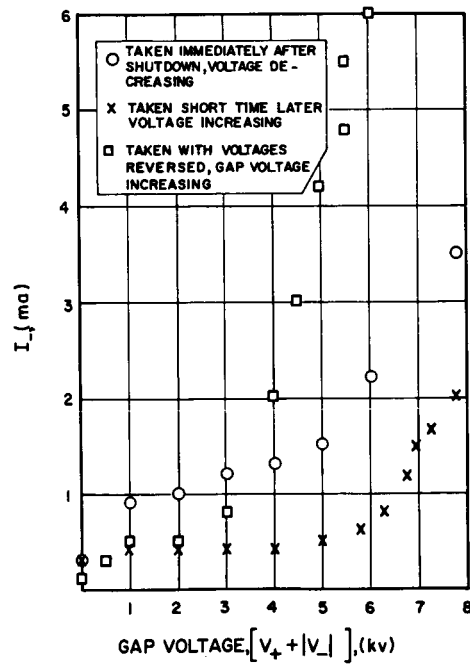


FIG. 2
RESIDUAL DRAIN CURRENT
VS GAP VOLTAGE FOR TWO
POLARITIES

Although not conclusive, the data and other information, to be discussed, led to the following hypothesis: With time, a composite Cs-O-Mo surface forms on the molybdenum accelerating electrode. The electrode temperature, surface conditions, and electric field are such that electron emission occurs. The electron current, accelerated across the gap, heats the screen electrode and engine and subsequently, by conduction and radiation, the accelerating electrode is heated which increases the electron emission. The drains then continue to increase to a high value by this mechanism.

Although the Malter effect may play a role, the main mechanism is probably field enhanced thermionic emission or the Schottky effect. Anomalities introduced by "patch effects" lead to the anomalous Schottky effect in which the current-voltage relationship may be such as that observed in Figures 1 and 2.

Accelerating electrode temperatures were measured for operating engines. For typical operating conditions, it was determined that the electrode temperature was about 300°C in the center and about 270°C at the periphery. At these temperatures, Schottky enhanced thermionic emission from a Cs-Mo surface would be much too small to explain the observed drain currents but emission from a Cs-O-Mo surface would be about 1000 times higher and in the right range. Experiments investigating the drain currents in contact cesium ion engines are reported in EOS Report 3830 Final, "Applied Research on Contact Ionization Thrustor", (APL TDR 64-52), pages 329-367. In these experiments it was found that under conditions in which the accelerating electrode temperature was at about 300°C, the admission of oxygen into the vacuum system increased the drain current by a factor of 5. This test was made with a copper electrode but the drain mechanism is probably the same.

The Cs-O-Mo surface exhibits high emission in an intermediate temperature range (perhaps 300-700°C). At lower temperatures the composite surface exists but the surface is too cool to give high emission. At higher temperatures, the composite surface is decomposed and the work function is too high to give high emission.

Other evidence exists that the drains are due to electron emission from the accelerating electrode. As the drains increase, the temperature of the cathode mounting plate at the rear of the engine is observed to increase. This is considered to be due to bombardment of the plate by some of the electrons accelerated across the accelerator gap. The high energy of these electrons (4-5 kev) is such that only a small fraction of the electrons need pass through the screen electrode apertures to provide the observed cathode plate heating.

2.2 Heated Molybdenum Electrode Test

A series of measurements of the accelerator drain current as a function of accelerator temperature were made to determine the effect of temperature and oxygen on the drain current.

For these tests a heater was brazed around the periphery of the hole pattern of a molybdenum accelerator electrode and a thermocouple was attached to the support point of the accelerator. A bleed valve was connected to the vacuum system for admission of air or oxygen.

The engine was operated at approximately 8 millipounds thrust with a screen to accelerator potential difference of 5000 volts. The reduced thrust level was used to allow the accelerator to operate below its normal operating temperature. The neutral efflux was adjusted to be equivalent to 40-50 ma corresponding to the neutral efflux under full thrust conditions. With steady state operation established the accelerator heater was turned on. Drain current was recorded as a function of temperature until the accelerator temperature reached 300°C. The heater was then turned off and drain current was recorded as a function of temperature until the initial operating conditions were regained.

The data obtained are shown by the circled data points in Fig. 3. The apparent hystereses in the data are probably due to slow changes in the equilibrium surface conditions on the accelerator and to a temperature difference between the emissive surface and the point at which the thermocouple was attached. The length of the support arm

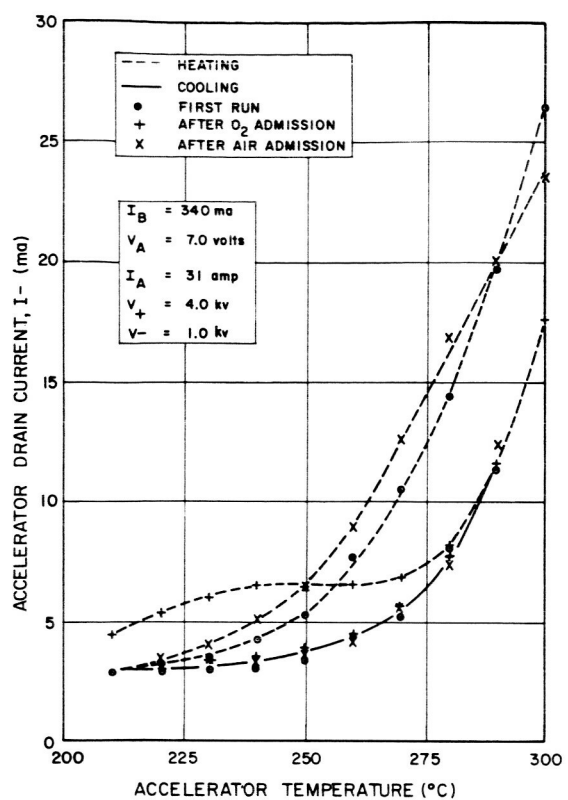


FIG. 3
TEMPERATURE AND OXYGEN
DEPENDENCE OF DRAIN
CURRENT

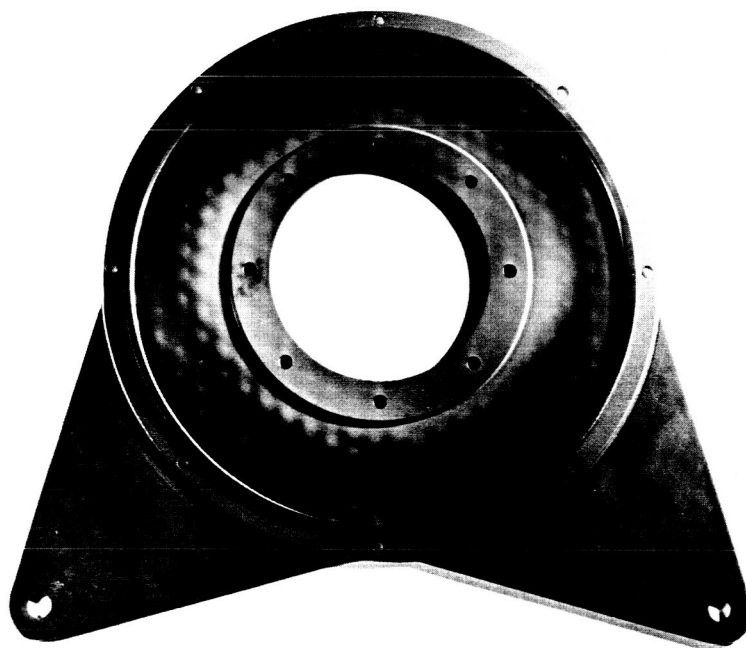


FIG. 4
CATHODE MOUNTING PLATE
AFTER HIGH DRAIN TEST

coupled with the heat capacity of the support insulator and shield should cause the measured temperature to lag the temperature of the electrode proper. A very strong temperature dependence is shown by the data of Fig. 3.

After returning to the original operating level, oxygen was admitted to the vacuum system until the pressure had risen from about 10^{-6} torr to 10^{-5} torr. A slight increase in drain current was noted as the pressure increased. When the pressure reached 10^{-5} torr, the bleed valve was closed and a sharp rise in drain current was observed. The system was allowed to regain the initial conditions and the heating and cooling test was repeated. The data obtained are shown by the crossed data points in Fig. 3. This data shows a significant increase in the drain current during the early portion of the heating cycle with no hysteresis apparent in the higher temperature data. The oxygen admission had apparently increased the electron emission at the lower temperatures. The heating above about 270°C , however, seems to have returned the electrode to its original surface condition.

A third set of data was taken after air was admitted to the vacuum system in a manner similar to the previous admission of oxygen. These data are shown by the X's in Fig. 3. This curve is quite similar to the curve obtained during the first run and indicates that the electrode surface had indeed been returned to its initial condition.

During all three tests, significant increases in cathode temperatures were measured when the drain current was high. At times, drain currents higher than 50 ma were observed. Upon disassembly of the engine, a pattern of "clean" spots was observable on the cathode plate which closely matched the electrode pattern. A photograph of this cathode plate is shown in Fig. 4. These spots are considered to be due to electrons accelerated through the screen apertures.

Some sources of error in this experiment must be considered. As noted above, of course, the measured temperature is in error to some degree. Secondly, the fact that these tests were performed sequentially

may have had some effect not discussed above. Finally, variations in the heating rates used could conceivably cause the results observed. This would not be a variable during the cooling portion of the tests. It must be concluded, since the cooling curves were identical, that either the original surface condition was regained after heating or the surface condition was not altered by the admission of pure oxygen. Finally, the conditions required to sustain the high drain currents at lower temperatures are elusive and even transient (high drain was encountered immediately after closing the oxygen valve) during short term testing.

The data do imply, however, that a molybdenum electrode designed to run at 230°C or less might not encounter the high drain conditions.

2.3 Cooled Copper Electrode Tests

Since the drain current situation appears to be particularly unfavorable for a molybdenum electrode, it was decided to test the engine with a copper electrode and to run it cooler by providing a large radiating area.

The cooled copper electrode is shown in Fig. 5. It was fabricated by brazing a DE design copper accelerating electrode to a 13 inch outer diameter heavy copper fin. The large copper ring was grooved to enhance its emissivity. When operated with an engine, this electrode had a temperature of 190°C at the periphery of the aperture pattern and an estimated 200°C at the center of the electrode. Due to distortion of the copper and close spacings outside the aperture area, engine operation was very noisy with much arcing. During 16 hours of operation, however, the drain current showed no increase.

The engine was reassembled with a 0.093 inch accelerating gap (measured at the center) instead of the normal 0.077 inch gap. Socket head cap screws in the screen electrode support structure were replaced with button head screws to further diminish the arcing problem of the previous run.

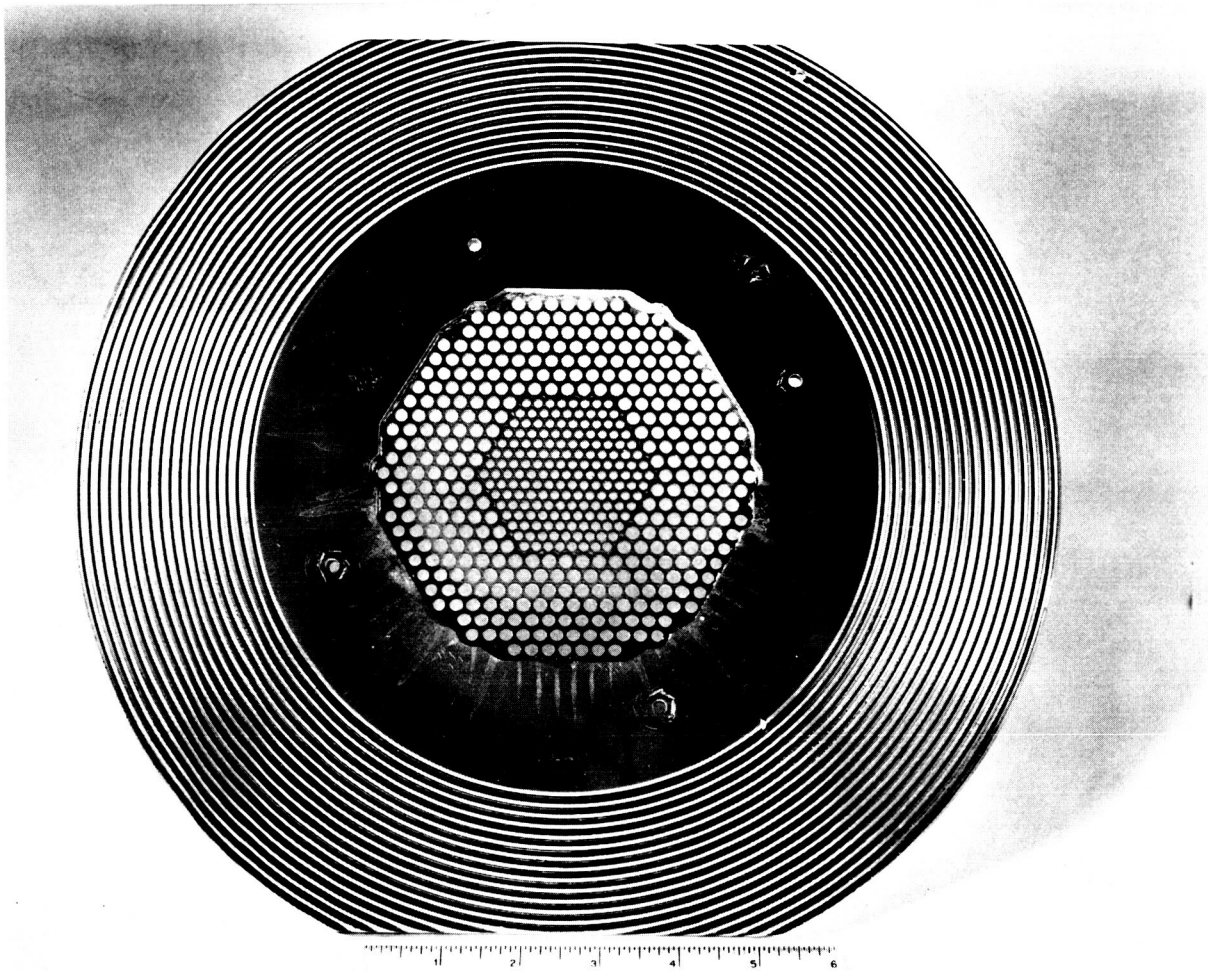


FIG. 5 COOLED COPPER ACCELERATOR ELECTRODE

With this electrode, and the larger spacings, an extremely stable beam with little or no arcing was achieved. The total run lasted 63.9 hours but was interrupted several times by vacuum system and negative high voltage supply malfunctions. The total accumulated operating time was 56.9 hours.

The engine was operated at a net accelerating potential of 4 kv and a beam current of 405 ma. During the run, the drain current stayed between 8.5 and 9.5 ma and showed no tendency to increase with time. The electrode temperature for previous tests with molybdenum electrodes was about 270°C measured at the same point.

The run was terminated by an increase in pressure in the vacuum system resulting from the decomposition of an insert in the Deutsch multi-pin power plug used with these engines. This decomposition occurred due to the excessive heat generated by the arc current passing through terminals in the plug. For subsequent tests, both anode and cathode (large current) power leads were re-routed directly to the engine so that they by-pass this plug.

Due to its massiveness no reliable weight could be obtained for the large copper electrode. After removal from the engine a visual inspection showed very little erosion due to sputtering of the electrode. Pits were noticed on the down stream side similar to damage noticed on other runs but the depth of these did not exceed a few mils.

3. LONG DURATION TEST

After the promising run with the cooled copper electrode the decision was made to perform a long duration engine test with a copper electrode of the normal DE design. A slightly larger than normal gap (0.083 inch versus 0.077 inch) was used to allow for thermal distortion. Consequently the perveance of the accelerator system was reduced. During the 297 hour test the engine was operated a total of 281 hours.

3.1 Operating Conditions and Time History

The vaporizer power history of the test is presented in Fig. 6. During the first 86 hours there were five interruptions due to high

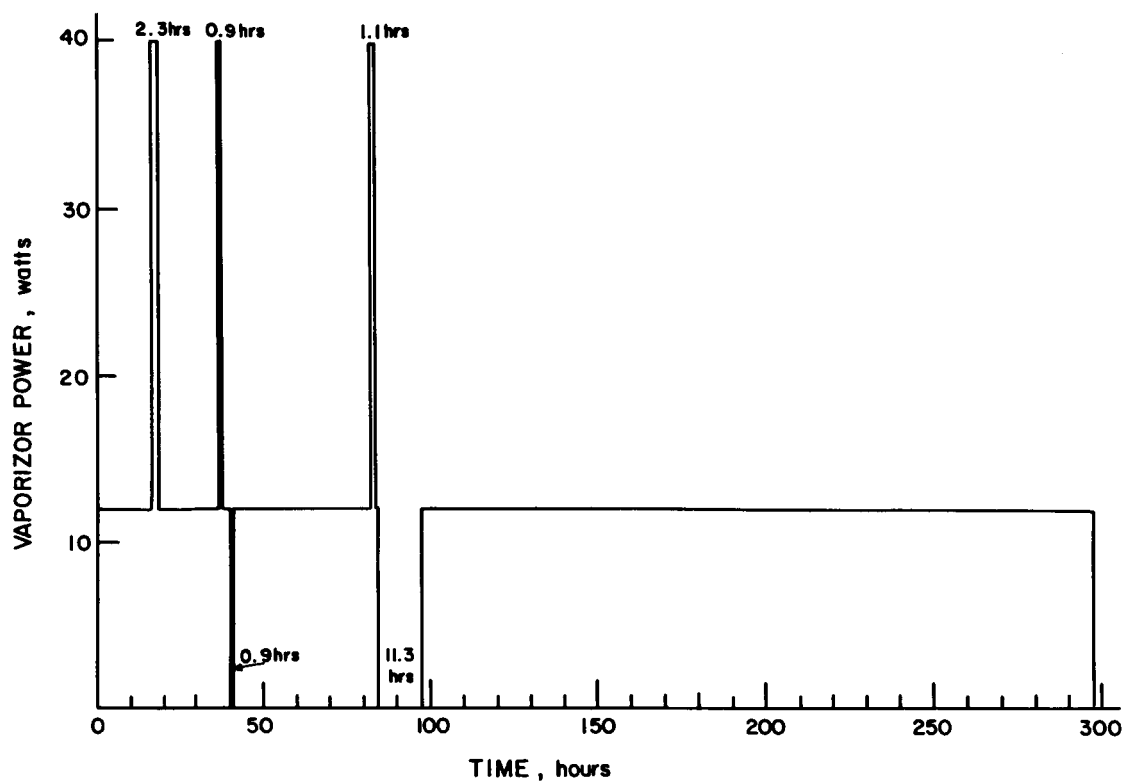


FIG. 6 VAPORIZER POWER HISTORY FOR 281 HR TEST

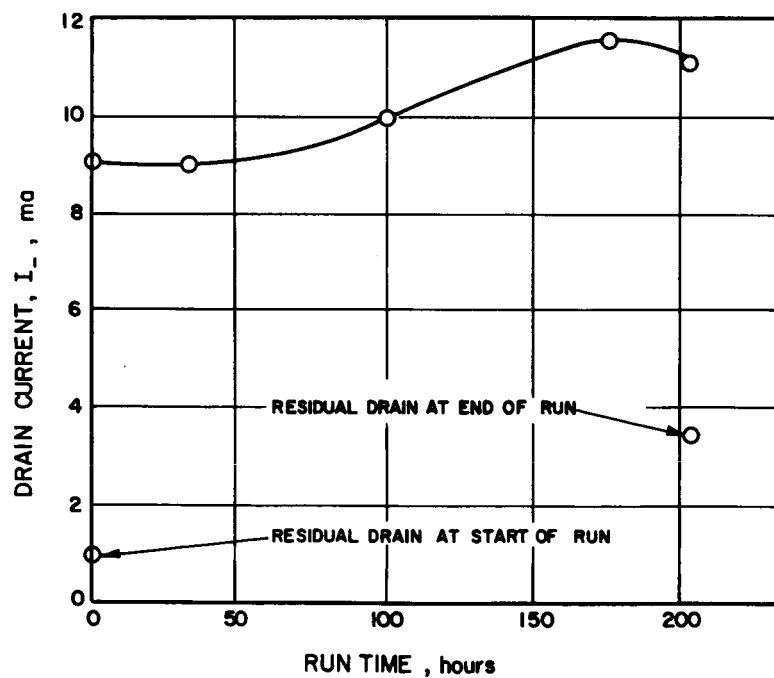


FIG. 7 DRAIN CURRENT VS TIME FOR 201 HR TEST

voltage overload circuit and cycling circuit malfunctions. Three of the interruptions resulted from a high voltage cycling relay sticking in a mode that kept high voltage turned off and provided a full beam demand signal to the feed control system. Consequently, during these off-periods, the vaporizer power was on full. Two of the interruptions were deliberate in order to attempt to fix the circuit components. During this phase the longest uninterrupted period of operation was 42.1 hours and the total accumulated operating time was about 80 hours. The test then proceeded with a 201 hour uninterrupted run. The total accumulated operating time was about 281 hours. The test was terminated on 7 August, 1964 with the engine operating normally. The drain current fluctuated about 2.5 ma but there was no significant increase other than in the residual insulator leakage current.

The engine operating parameters during the 201 hour continuous segment of the test are presented in Table I. Three points are shown indicating the trend with time. Small changes were made in the high voltage and arc power settings to minimize drain during the course of the run. The drain current increased from 9 to 11.5 ma during the 201 hour period while accelerator electrode and cathode temperature were on a downward trend. Since arc power was adjusted down from time to time this would explain the decrease in the above temperatures. Figure 7 shows the gradual drain increase with time; it also shows the residual drains taken immediately preceding and after the continuous run. With the arc extinguished and the electrodes cool, the residual drain at the start was approximately 2.5 ma below the drain at the finish (1.0 ma versus 3.5 ma). This indicates that the increase was due to insulator leakage and not electron emission.

It was assumed that the high operating level of the drain current (over 2 percent of beam) was due to misalignment of the accelerator electrode as a jig was not used in assembly of the electrode structure. Inspection after the test revealed a non-concentric erosion pattern on the outer holes of the accelerator electrode in substantiation of the misalignment assumption.

TABLE I
Engine Operating Parameters
During 201 Hour Continuous Test

<u>Run Time (hours)</u>	<u>34</u>	<u>100</u>	<u>175</u>
Positive High Voltage, V_+ (kv)	4.2	4.2	4.2
Negative High Voltage, V_- (kv)	.75	.60	.55
Negative HV Current, I_- (amp)	.009	.010	.0115
Beam Current, I_B (amp)	.405	.402	.402
Arc Voltage, V_A (volt)	7.7	7.6	7.5
Arc Current, I_A (amp)	41.0	40.5	40.5
Beam Power, P_B (kw)	1.701	1.689	1.688
Drain Power, P_D (kw)	.045	.048	.055
Magnet Power, P_M (kw)	.008	.008	.008
Arc Power, P_A (kw)	.316	.308	.304
Total Power, P_T (kw)	2.070	2.053	2.055
Thrust, T (mlb)	9.89	9.81	9.81
Power-to-Thrust, P/T (kw/lb)	209	209	210
Power Efficiency, η_p	82.2%	82.5%	82.2%
Mass Efficiency, $\eta_M \sim$	90%	90%	90%
Overall Engine Efficiency, η_E	74.0%	74.2%	74.0%
Specific Impulse I_{sp} (sec)	7160	7160	7160
I_-/I_B	2.2%	2.5%	2.9%
P_A/I_B (kev/ion)	.780	.766	.756
Pressure (mm Hg)	2.2×10^{-7}	2.4×10^{-7}	1.8×10^{-7}
Operating Temperatures ($^{\circ}\text{C}$)			
Accelerating Electrode	306	305	304
Engine Shell	306	301	309
Cathode Housing	440	425	428
Vaporizer	251	243	250

Vaporizer power ran at 12.1 watts throughout the run with vaporizer temperature at 250°C; variations in these values were less than 3 percent. It should be noted in Table I that the copper electrode runs hotter than does a molybdenum electrode. This is due to the lower emissivity of copper since much of the electrode heating appears to be by conduction across the electrode support insulators. A low thermal conductivity path in either the engine shell side of the insulator or the accelerator electrode side of the insulator would allow operation at significantly lower electrode temperature. This idea will be incorporated into future engine designs.

The test can be summarized as one with little or no unexplainable drift in any of the measured parameters and with very stable operation.

A liquid nitrogen cooled neutral detector, used at the start of the run, gave a mass utilization efficiency of 90 percent. At the end of the run a mass utilization efficiency of 90.6 percent was obtained. During the full 297.5 hours of the test, 776.2 gms of cesium were expelled. In the 4.3 hours of time during which high voltage was off and vaporizer power was on full, it was estimated that the flowrate was equivalent to 6 to 9 amperes of cesium ions. This was based on flowrate versus vaporizer power tests conducted under previous programs. It is therefore estimated that over 150 gms cesium were lost to the system during these periods and that about 620 gms were consumed during engine operating periods. This is in agreement with the mass utilization measurements which indicate a total of 624 gms cesium were expelled excluding start-up periods and high vaporizer power periods.

3.2 Residual Drains

At the termination of the 281 hour test, the accelerating electrode temperature and the drain current were monitored. Figure 8 presents these parameters as a function of time after termination of the run. The high voltages were maintained during the procedure. As can be seen, after the electrode was quite cool (185°C), a residual drain of 3.5 ma remained. This is considered to be an insulator drain current.

The residual drain current was then measured as a function of voltage across the accelerating gap. The temperature of the electrode was about 185°C at this time. The data are presented in Fig. 9. Each time the original voltages were applied (as indicated by the squares) the drain returned to 3.5 ma.

The voltages applied to the arc chamber and the accelerating electrode were then reversed and reversed polarity data was taken. The data are presented in Fig. 10. The test indicates the existence of electron emission from the molybdenum screen electrode which was at about 200°C when the data was taken. The data indicated by X's, for the gap voltage decreasing, was plotted as a Schottky plot shown in Fig. 11. As can be seen in the figure, a quite linear relation exists between the logarithm of the current and the square root of the voltage (or field intensity).

Extrapolation of the Schottky plot indicates a thermionic current requiring a work function of less than 1.2 ev. The Cs-O-Mo composite surface appears to exist on the molybdenum screen electrode.

The field between flat parts of the screen and accelerating electrodes is on the order of 10,000 volts/cm at 2.2 kv across the gap. The slope of the Schottky plot requires a field over 100 times more intense. Perhaps the field at the sharp edges of the apertures in the screen electrode are large enough to account for the large Schottky enhanced emission. The downstream sides of the apertures were not radiused.

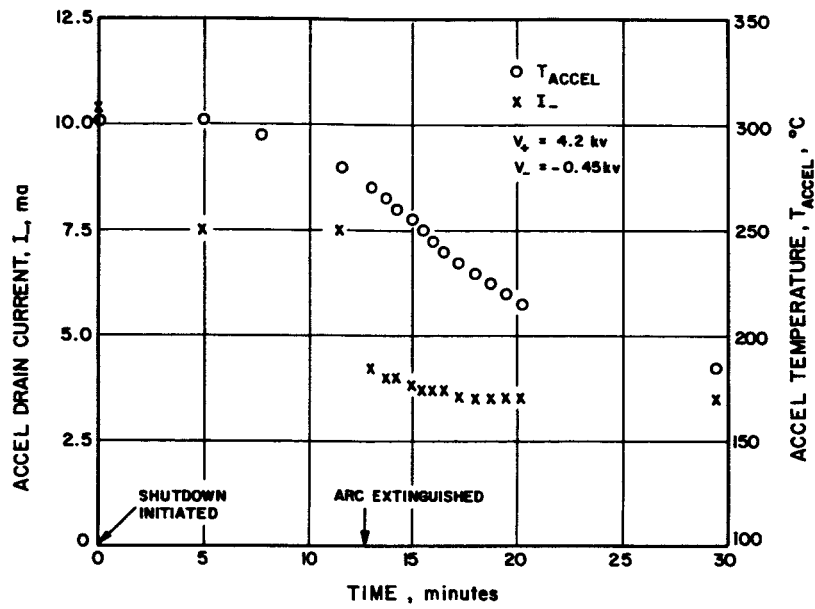


FIG. 8 ACCELERATING ELECTRODE TEMPERATURE AND DRAIN CURRENT AFTER TEST TERMINATION

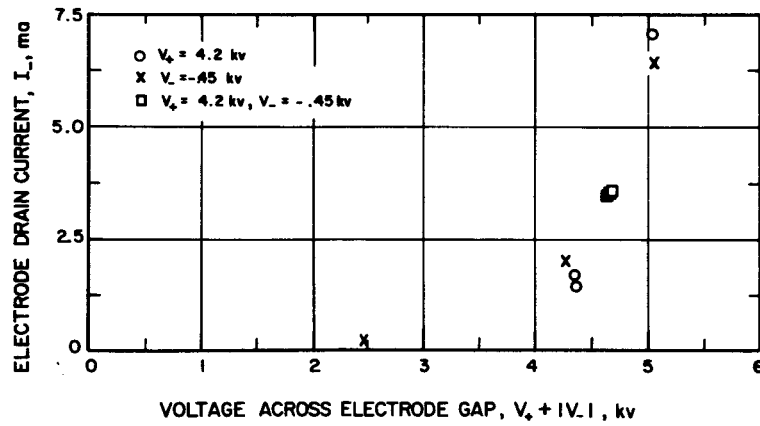


FIG. 9 ACCELERATOR DRAIN CURRENT VS GAP VOLTAGE

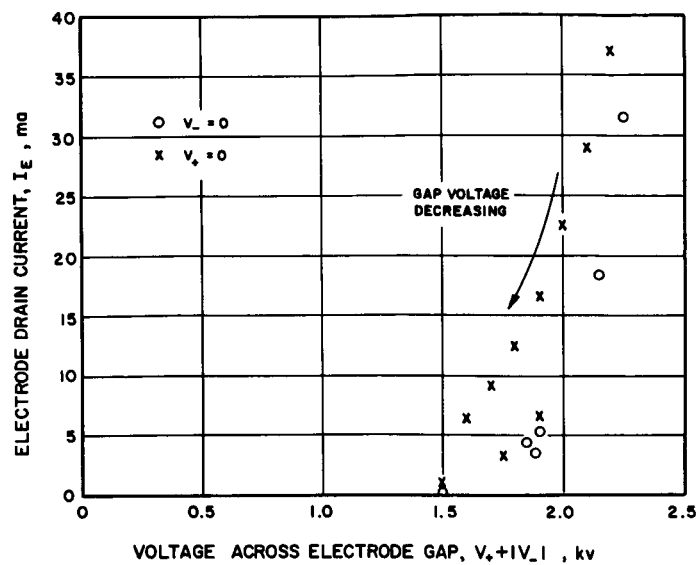


FIG. 10 DRAIN CURRENT VS GAP VOLTAGE FOR REVERSED POLARITY TEST

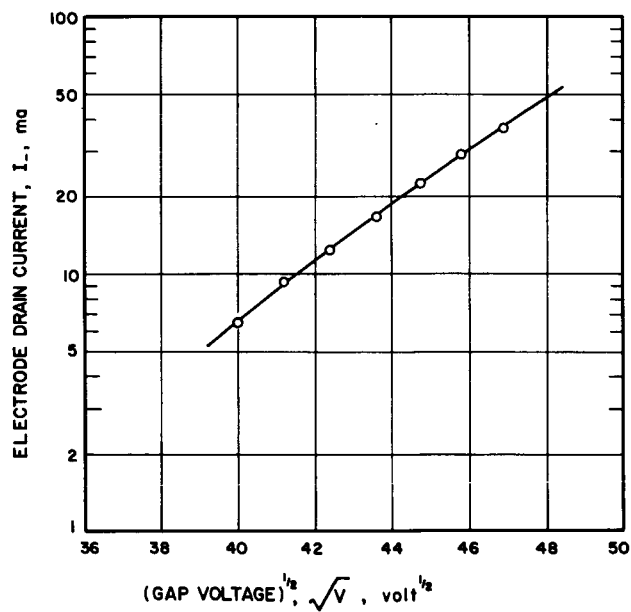


FIG. 11 SCHOTTKY PLOT FOR REVERSED VOLTAGE TEST

3.3 Condition of Engine After Test

A pictorial record of the system and components immediately after the run can be seen in Figs. 12 thru 19. The engine system, shown in Fig. 12, was extremely clean. Only copper (on areas facing the collector) was visible upon inspection. Figure 13 is a view of the inside of the cathode and orifice plate. They both appeared in excellent condition. A light deposit was found on the first two coils next to the baffle (see photo) which appeared to be either residue from impurities in the propellant or from the braze compound. Unfortunately, not enough of this substance could be obtained to be analyzed.

There was a non-uniform heating pattern on the orifice plate. A similar off-center, light area was found on the up-stream side of the accelerator electrode. This condition has been noted before. The clean area at the cathode is due to electron heating. Since the clean areas on both parts are in line with each other it would appear that the emission was occurring from the clean spot on the electrode.

Figure 14 shows the inside of the arc chamber. The chamber and cathode plates were copper coated to thicknesses up to .001 inches. Note the distorted electrode hole pattern on the front portion of the anode. This is due to copper sputtered back from the liner and collector passing through the electrode system.

The most severe damage to the engine occurred on the outer shell (magnet cover) where electron bombardment had worn through the .003 inch thick titanium sheet. This might have damaged the magnet coils had the run continued. Careful inspection of Fig. 15 reveals one of these thin spots on the lower front cover. It would appear that some electrons from the beam plasma were focused to these spots.

There was a 2 to 3 inch wide annular gap between the engine and the front of the ground cage. The placement of the negative high voltage lead was such as to focus backstreaming electrons to spots on the shell on both sides of the negative lead. The damage by backstreaming electrons can be easily eliminated by removing these negative leads from the area between the engine and ground shield and by a closing in

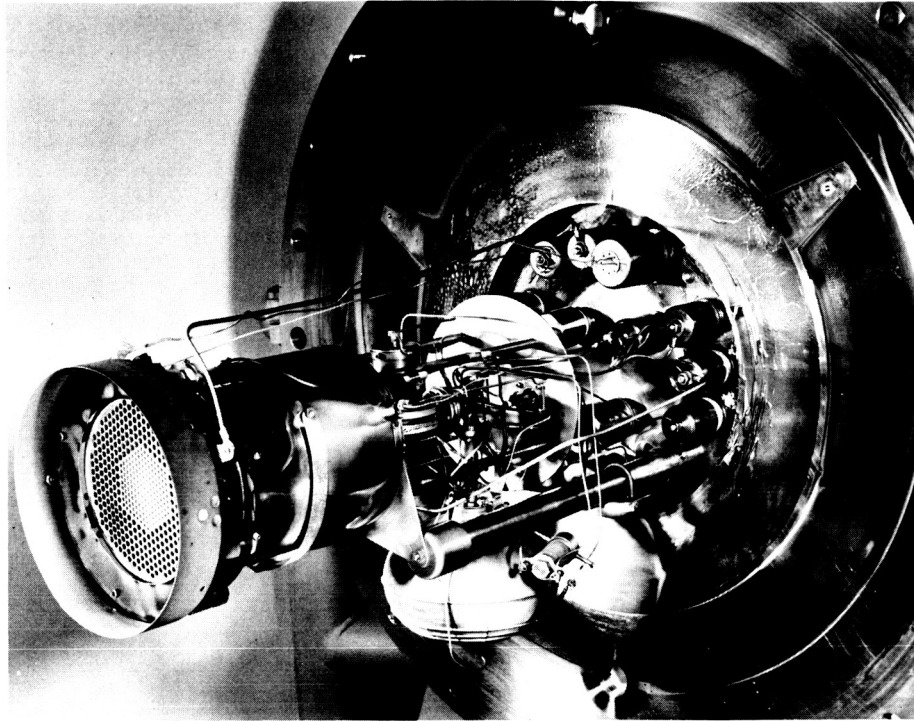


FIG. 12 DER-1 ENGINE SYSTEM AFTER 281 HR TEST

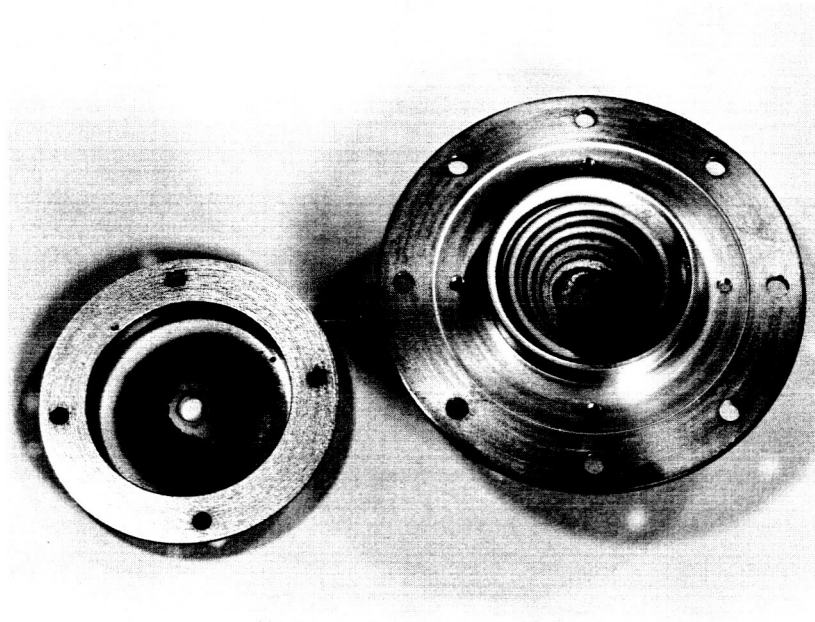


FIG. 13 CATHODE AND ORIFICE PLATE

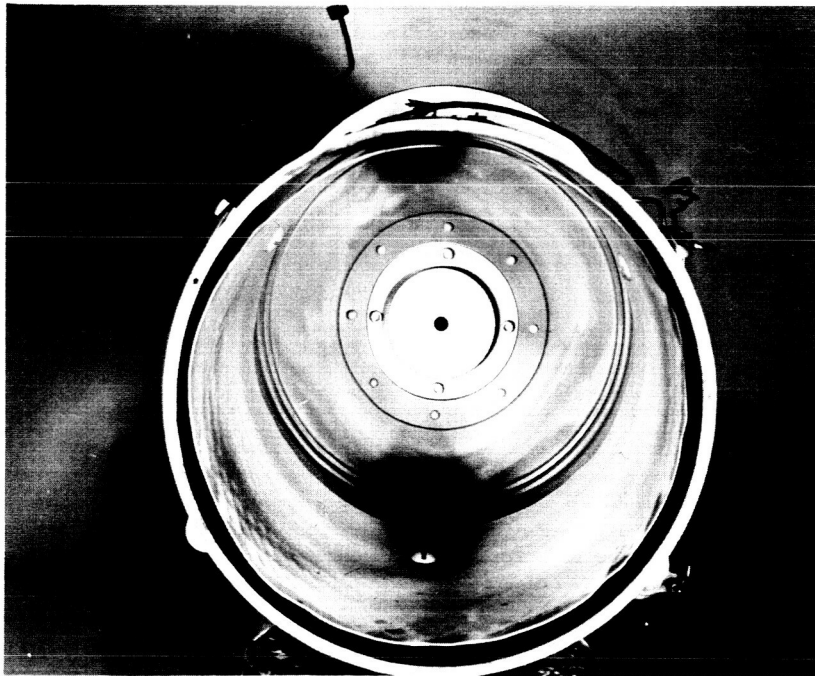


FIG. 14 ANODE AND CHAMBER INTERIOR

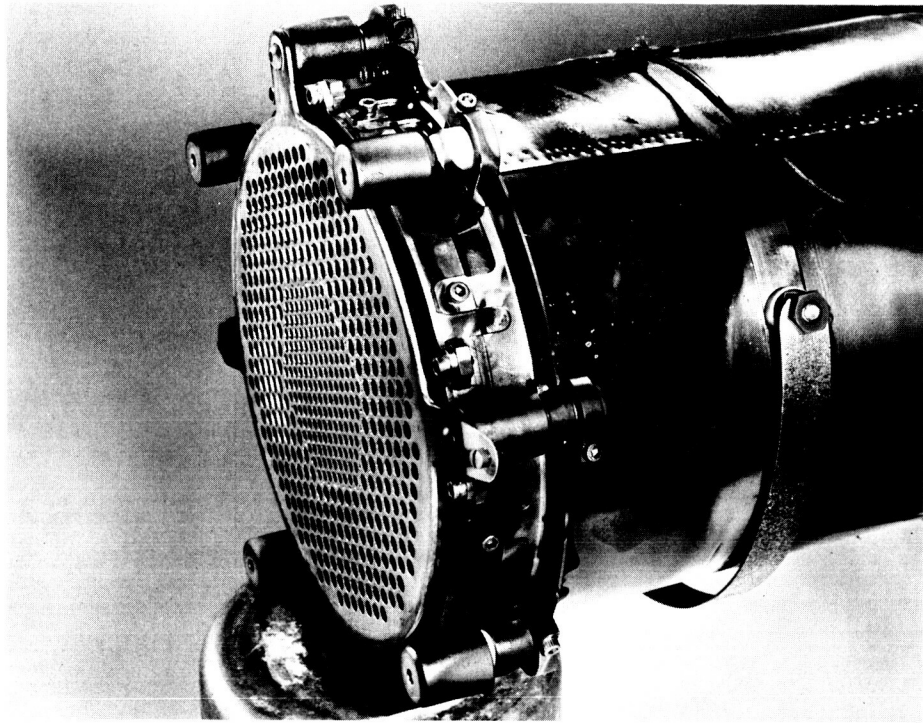


FIG. 15 ENGINE SHELL

the ground cage.

Figure 16 indicates the condition of insulators after the run. They appeared relatively clean under the shielded area although localized dark rings could be found in the troughs of the convoluted surfaces. In general the hotter the running temperature, the cleaner the surface. Unshielded parts of the insulators were contaminated.

The screen electrode was discolored but no visible erosion was noted. Figure 17 is a view of the electrode assembly showing the upstream side of the screen. Note the discoloring in the grid portion and the metallic appearance of the outer edge of this plate. The small lip machined on these plates is successfully preventing cesium from escaping through this joint.

All wiring and connectors including Deutsch plugs seemed in excellent condition with no observable loosening of the joints.

Accelerating Electrode

Figure 18 is a photo of the downstream side of the accelerating electrode. The major erosion occurred on the webbing between large and small holes. Depth of the pits at this interface and at positions along six equally spaced radial lines from the electrode center were measured. The deepest pits were in twelve locations, where a large web area results from the change in hole patterns. The depth of these pits ranged from .0184 to .0238 inches. A photo-micrograph of a sample section through one of these pits appears in Fig. 19.

Depth of pits in the small hole pattern ran from .0048 to .0139 inches with the deepest holes nearer the outer part of the pattern. Pits in the large pattern ran from .0099 inches at the inside of the pattern to no pits at the outer edge. A photo-micrograph of one of the shallow pits appears in Fig. 20. Figure 21 shows the upstream side of the accelerator electrode. There was no visible erosion.

Copper deposited on the downstream side of the electrode was .00062 inch thick. The estimated weight of this layer is 1.1 gm.

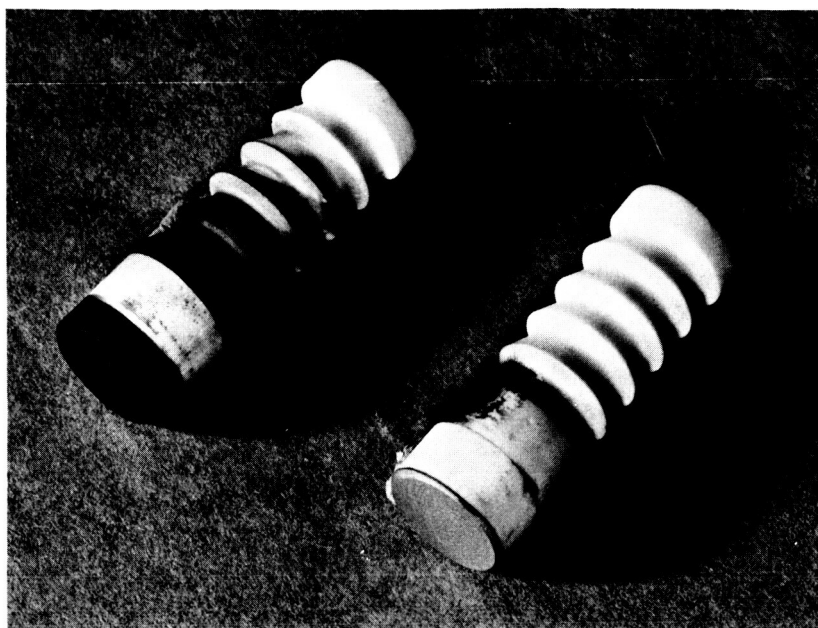


FIG. 16 INSULATORS

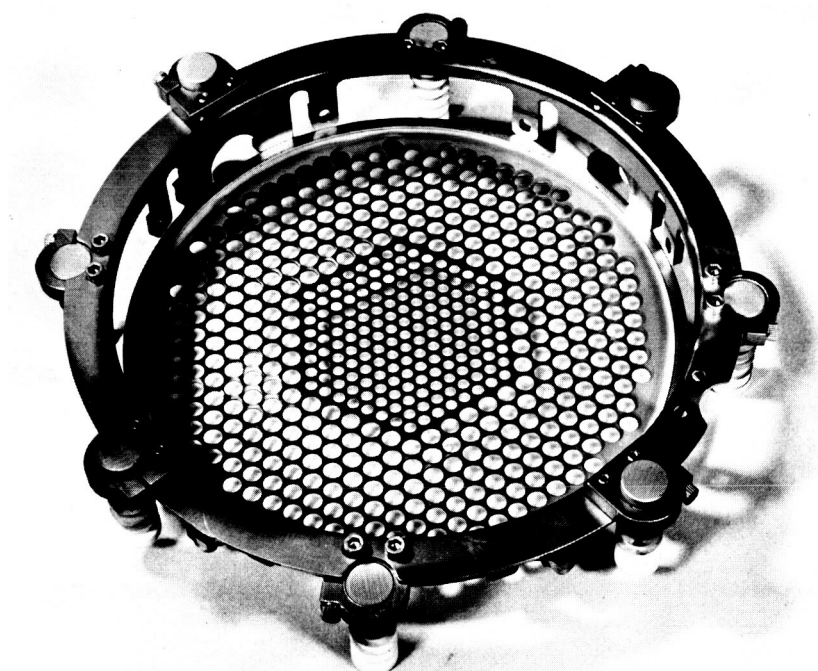


FIG. 17 SCREEN ELECTRODE

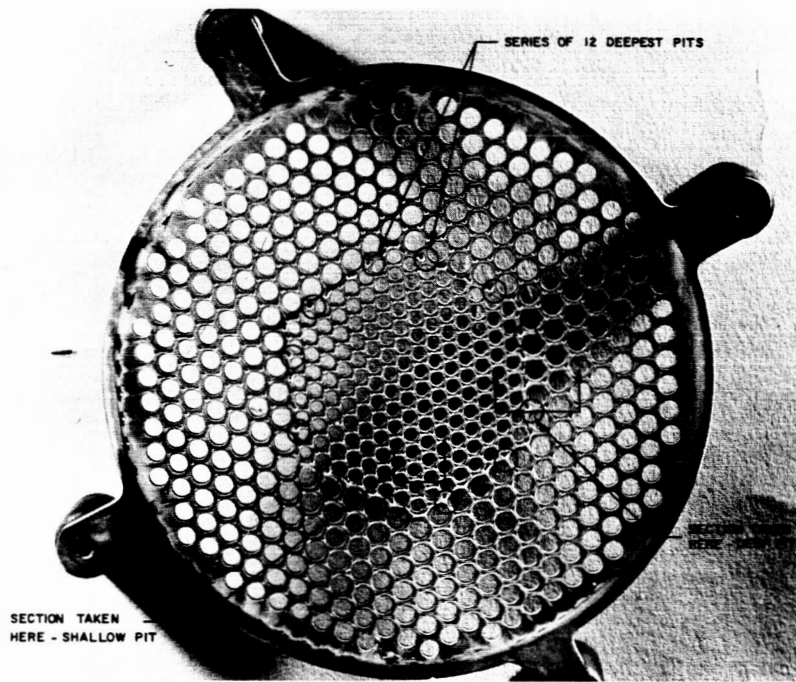


FIG. 18 ACCELERATING ELECTRODE - DOWNSTREAM SIDE

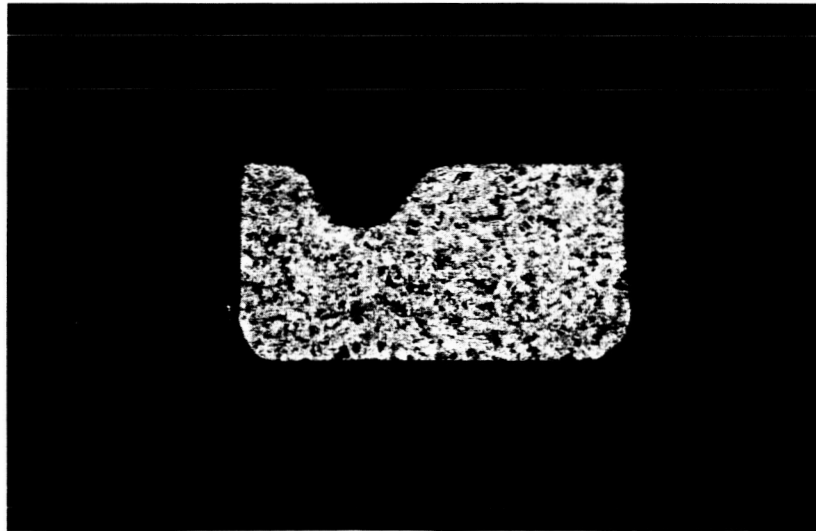


FIG. 19 CROSS SECTION OF DEEP PIT

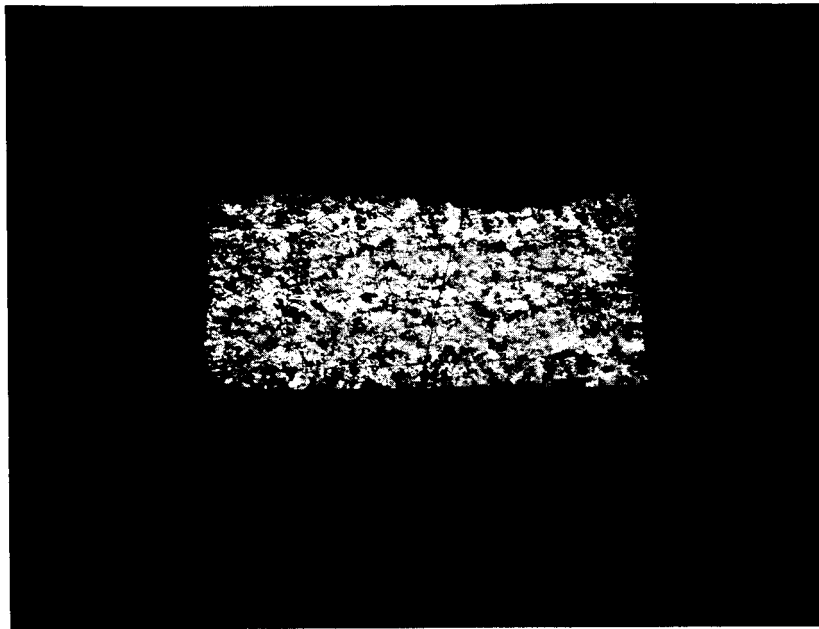


FIG. 20 CROSS SECTION OF SHALLOW PIT

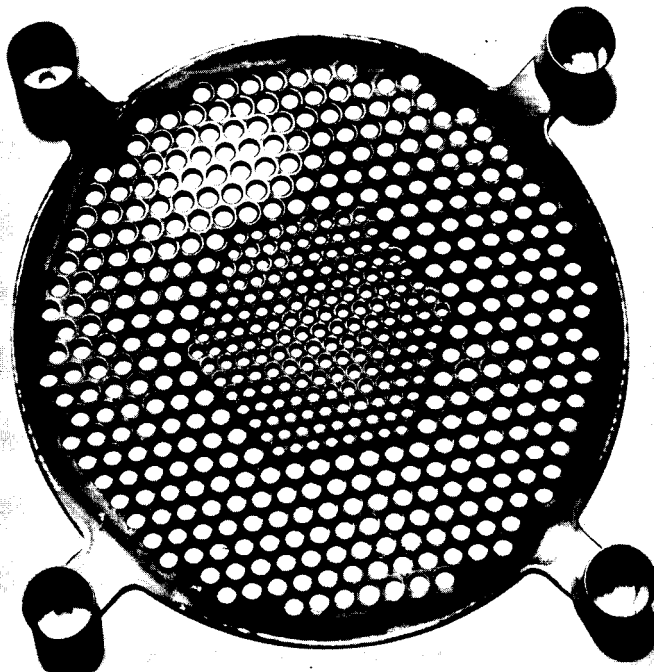


FIG. 21 ACCELERATING ELECTRODE - UPSTREAM SIDE

Adding this to the weight loss of the electrode after the run indicates a total weight loss, during 281 hours of operation, of 2.25 gm.

Several holes were eroded on one side indicating the misalignment due to visual adjustment; as mentioned earlier this was a contributing factor to high drain.

It is possible that this electrode could be run for a few thousand hours. Even when the twelve deep pits had eroded through, the structural rigidity would have remained.

Sample Analysis

Scrapings were taken from various components and sent out for chemical analysis. A summary of the results is presented in Table II. Only a qualitative analysis is meaningful due to the lack of knowledge regarding the amount of base material taken into the sample

Small amounts of silicon appeared in all the samples and this is attributed to diffusion pump oil which contains this element. Similarly, copper was found on all components and as mentioned earlier this material was sputtered back to surfaces facing the collector. The upstream side of the screen electrode which does not face the collector, apparently collected copper evaporated off the cathode plate and orifice.

The molybdenum on the anode and on the upstream side of the accelerator electrode probably came from the molybdenum orifice plate as this part had lost weight during the run. Gold was located on both the anode and screen. The only gold in the system is found in the braze material used to fasten cathode parts.

The single result that is difficult to explain is the presence of molybdenum on the downstream side of the accelerator electrode. Since molybdenum was leaving the cathode orifice plate and probably the cathode, part of it must have reached the collector. This may have been sputtered back to the engine.

Weight Changes

Weight of the critical parts before and after the run are presented in Table III and the gains and losses indicated.

TABLE II

Analyses of Deposits on Components

<u>Component</u>	<u>Base Material</u>	<u>Major Contaminant</u>	<u>Other Significant Contaminants</u>
Accelerating Electrode (Downstream)	Copper	Molybdenum (small amount)	Silicon
Accelerating Electrode (Upstream)	Copper	Molybdenum	Silicon
Screen Electrode (Downstream)	Molybdenum	Copper	Silicon
Screen Electrode (Upstream)	Molybdenum	Copper	Gold Silicon
Anode (Inside Front)	Copper	Molybdenum	Gold Silicon
Cathode Orifice Plate (Downstream)	Molybdenum	Copper	Silicon

Very small traces (<0.01%) of iron, titanium, and aluminum were detected for all samples.

TABLE III

Component Weight Changes

Component	Weight Before Run (gms)	Weight After Run (gms)	Weight After Cleaning (gms)	Net Change (gms)	%Change
Accelerating Electrode	141.9354	140.7920		-1.1434	-0.80%
Screen Electrode	119.2758	119.6846	118.8092	-0.4666	-0.04%
Anode	349.6603	350.7488	350.2770	+0.6167	+0.02%
Cathode Orifice Plate	26.4270	26.4854	26.3614	-0.0656	-0.25%
Cathode Mounting Plate	135.4051		135.3540	-0.0511	-0.04%

It is difficult to say how much error is introduced into the determination of these net weight changes by the cleaning processes. Care was exercised to remove only coatings but base material was found in most samples.

Since the anode is made of copper and since no photo-micrographs were taken the added weight due to plating was not determined. The cleaning process did not remove all of the plating; thus the gain in weight.

4. FEED SYSTEM

4.1 Analysis of Feed System After Test

Following the 281 hour duration test, the zero-g feed system was completely dismantled and an analysis made on many of the components. The feed system was disassembled in the dry box. The photographs of Figures 22, 23, and 24 show the components of the system while still in the dry box. It was observed that the cesium both in the reservoir and on the porous rod was clean and bright. Slight discolorations were noted in the vaporizer tube and on the valve body. The valve ball contained a small deposit of material. Analysis of this deposit disclosed copper, gold, and silicon as the contaminants. Sectioning of the reservoir showed it to be exceptionally clean inside with no evidence of cesium corrosion or attack at weld joints or on the fin assembly.

The porous rod was sectioned while still in the dry box. Five samples were removed for analysis. Figure 25 indicates the location on the porous rod where samples were removed. Table IV lists the results of the quantitative spectrographic analysis that was performed on these samples. Included in this table is the analysis of a control sample which was removed from the same porous rod prior to the engine run.

A sample of the remaining cesium was also obtained during the disassembly. An analysis of this sample is compared with a sample that was obtained during the initial filling operation and is shown in Table V.



FIG. 22 FEED SYSTEM COMPONENTS

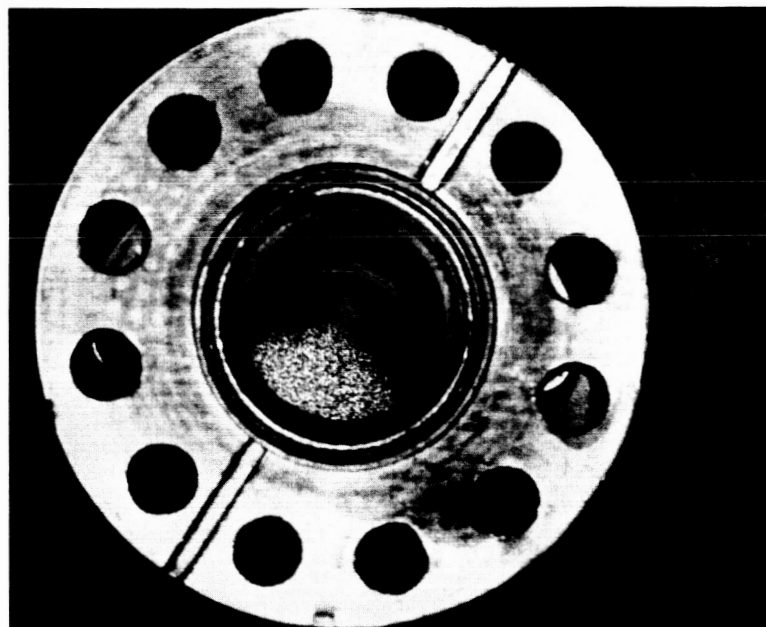


FIG. 23 END VIEW OF VAPORIZER SURFACE

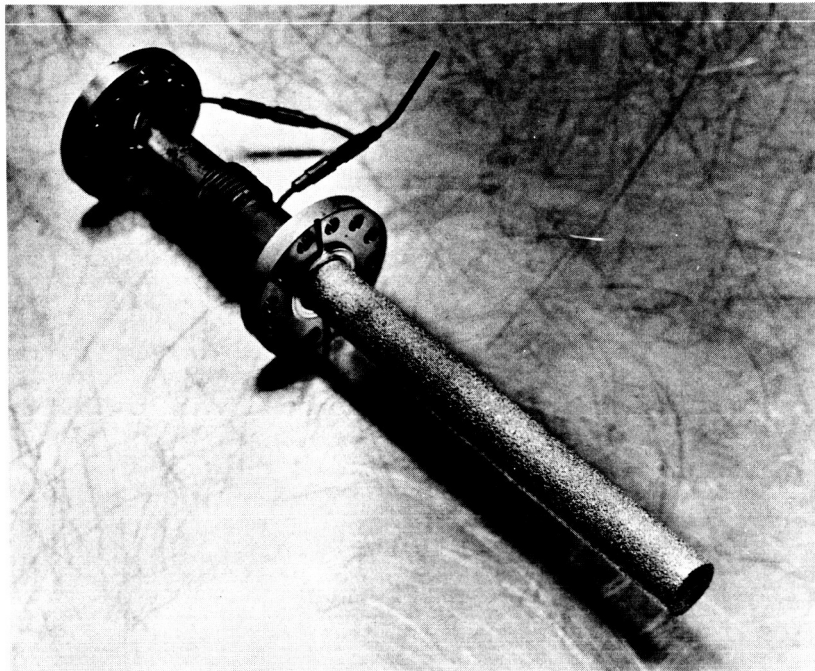


FIG. 24 POROUS ROD AND VAPORIZER ASSEMBLY

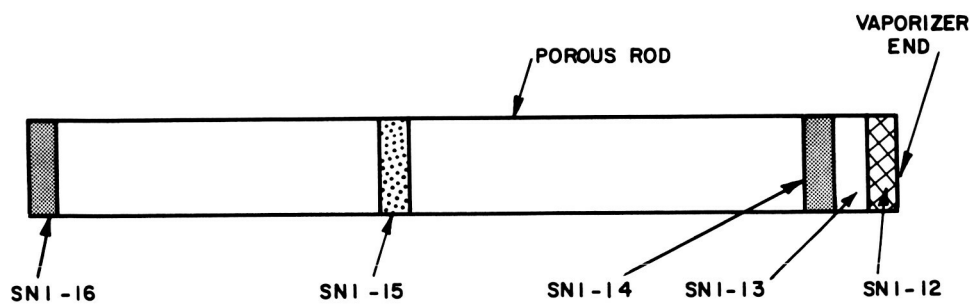


FIG. 25 LOCATION OF SAMPLES TAKEN FOR ANALYSIS

TABLE IV
Analysis of Porous Rod

<u>Element</u>	<u>Control Sample SN1-11</u>	<u>SN1-12</u>	<u>SN1-13</u>	<u>SN1-14</u>	<u>SN1-15</u>	<u>SN1-16</u>
Manganese	.09%	.01%*	.01%*	.01%*	.01%*	.02%*
Iron	.38%	.09%	.03%	.12%	.10%	.11%
Silicon	.10%	.17%	.13%	.12%	.11%	.18%
Copper	.03%	.15%	.08%	.10%	.13%	.09%
Cobalt	.16%	.11%	.09%	.12%	.15%	.13%
Titanium	.03%	.01%*	.01%*	.01%	.02%	.03%
Magnesium	.06%	.12%	.05%	.06%	.02%	.11%
Nickel	Rem.	Rem.	Rem.	Rem.	Rem.	Rem.

* Less than

TABLE V

Analysis of Cesium Samples

Element	Sample	
	Before Run	After Run
Cesium -----	Remainder	Remainder
Aluminum -----	1 PPM*	1 PPM*
Barium -----	20 PPM*	20 PPM*
Boron -----	10 PPM*	10 PPM*
Calcium -----	10 PPM	1 PPM*
Chromium -----	1 PPM*	1 PPM*
Iron -----	13 PPM	1 PPM*
Magnesium -----	1 PPM	.5 PPM
Manganese -----	1 PPM*	1 PPM*
Nickel -----	1 PPM*	1 PPM*
Lead -----	25 PPM	7 PPM*
Tin -----	35 PPM	15 PPM*
Strontium -----	2 PPM*	1 PPM*
Lithium -----	20 PPM*	20 PPM*
Titanium -----	3 PPM*	3 PPM*
Thallium -----	3 PPM*	3 PPM*
Sodium -----	5 PPM*	5 PPM
Potassium -----	10 PPM*	10 PPM*
Columbium -----	20 PPM*	-
Molybdenum -----	3 PPM*	-
Silicon -----	8 PPM	1 PPM*
Copper -----	1 PPM	1 PPM

* less than
- not detected

After removal from the dry box, the reservoir was sectioned. Two sections of the peripheral weld were obtained. Photo-micrographs at a magnification of 400X are now in process to determine if any intergranular corrosion has occurred at the weld. Photo-micrographs will also be obtained on a section of the vaporizer tube and on one of the fins to compare with similar photo-micrographs made before the run on the same fin. Also a sample of this fin was taken for spectrographic analysis and will be compared with an analysis made on the same fin during the feed system assembly. The results of the photo-micrographs of the welds and fin and the analysis of the fin will be reported in the next monthly report.

Finally, weight and dimensional measurements were obtained on many of the feed system components. These are compared with measurements obtained during the assembly period. The results are tabulated in Table VI.

An examination of the various analyses and measurements shows no significant changes in cesium purity, no evidence of harmful clogging of the porous rod, and no significant weight or dimensional changes. In short, it appears that this system will easily meet the goals of the program and provide propellant to the engine for its full capacity of 750 hours.

4.2 Feed System Improvements

Manually Operated Cesium Valve

The zero-g feed system used in the engine tests has response characteristics sufficiently fast to accommodate all of the engine control requirements. A valve is required only to provide a barrier which protects the cesium when the feed system is not in the vacuum environment of the test chamber. Therefore, it need only be opened before the engine is started and closed before the engine is removed from the chamber. Currently, a solenoid valve is being used for this purpose and operation has so far been satisfactory. The reliability of the solenoid valve for long runs is not certain, however, and the

TABLE VI
Weights and Dimensions
of Feed System Components

Part	Before run	After run
	weight (grams)	
Port Valve	124.9107	125.7148
Fin Assembly	434.8170	431.2212
Control Fin	5.5573	5.5088
Vaporizer	91.8317	91.7929
Elbow	108.0323	107.9283
<u>Valve</u>		
Body	318.1662	317.9129
Diaphragm Assy.	40.6733	40.5964
Ball	.8062	.8029
<u>Copper Seals</u>		
Reservoir-Vaporizer	1.7846	1.7859
Vaporizer-Elbow	1.7879	1.7888
Elbow-Valve	1.7852	1.7859
Reservoir-Port Valve	1.7994	1.7974
Solenoid Valve Seal	9.4582	9.2594
	dimension (inches)	
Reservoir Shell Thickness (top)	.0307	.0305
Reservoir Shell Thickness (bottom)	.0317	.0315
Control Fin Thickness	.005	.005
Heater Bore Diameter	.4905	.491

possibility of a run having to be terminated due to a valve failure should be minimized. A manual valve is therefore considered to be desirable.

A mechanical cesium vapor valve was designed and fabricated during the quarter. It is for use in place of the existing solenoid valve on the DER engine system. Its purpose is to provide a reliable leak-tight valve for laboratory testing. Some interesting features of the valve which is shown in Figures 26 and 27 are described below. The valve consists of three sub-assemblies; the valve body, the poppet assembly, and the actuating mechanism. The valve body is fabricated of type 347 stainless steel and heated with a sheathed heater. Its mass is considerably less than the mass of the solenoid valve which is currently being used. It is expected that heat-up times will therefore be considerably shortened.

The poppet assembly consists of the valve poppet which is welded to a metal diaphragm similar to that used on the solenoid valve. The only seal used in the valve is between the body and poppet assembly. The actuating mechanism is of hardened type 17-4 stainless steel. The screw mechanism is overcoated with a high temperature solid-film lubricant to minimize friction. In addition, thermal isolation is provided between the actuating assembly and the valve body to minimize heat conduction to the actuating assembly.

Actuation of the valve is provided by a retractable rod which is introduced through the vacuum flange. An O-ring assembly on the flange prevents leakage at the flange. Since the rod is retracted when high voltage is applied to the engine, there is no need for electrical isolation of the rod.

Testing of this valve had included helium mass spectrometer leak checking and room temperature cycling. Twenty successive actuations were made with no detectable leak across the valve. The detector used has a sensitivity of 10^{-10} std cc He/sec. Actuating torque during this test was held constant at 25 inch-pounds. The valve was assembled to a feed system and cesium flow tested at valve body temperatures up

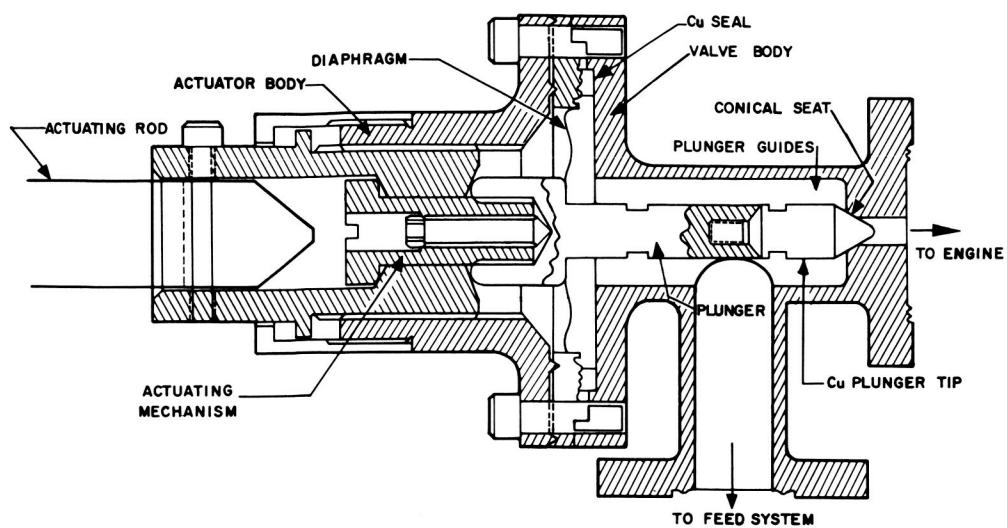


FIG. 26 MANUALLY OPERATED CESIUM VALVE

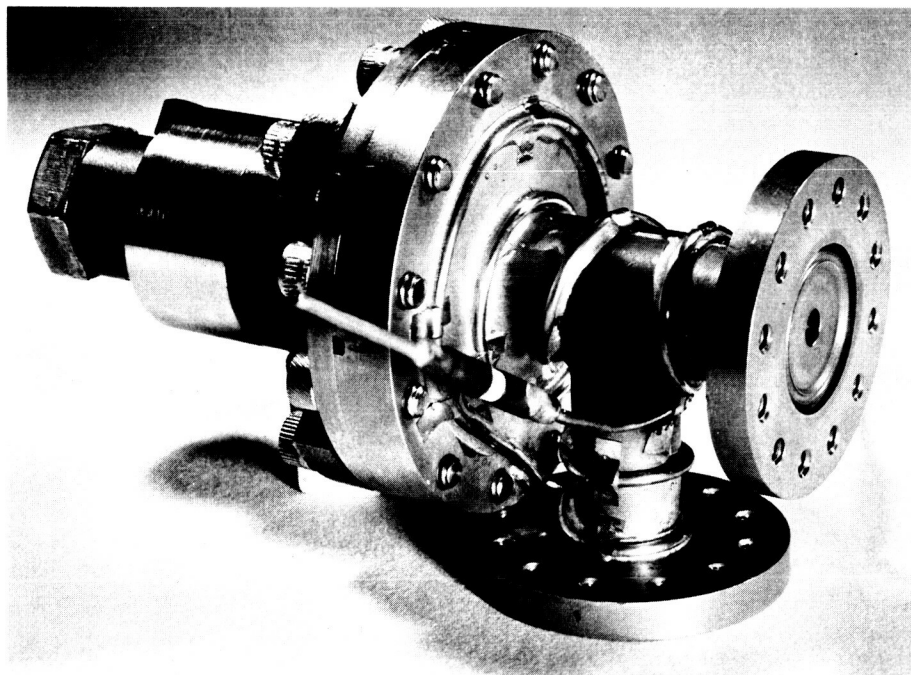


FIG. 27 MANUAL VALVE

to 400°C. All tests have been satisfactory.

Pump-Out Valve

Another area of improvement is the rear pump-out valve on the cesium reservoir. A new pump-out valve has been designed and fabrication started. The main purpose for a redesign here was to provide a valve with a larger orifice. The existing pump-out valve has a port orifice diameter of only 1/16 inch. This small orifice size is easily obstructed by any cesium that might deposit there due to distillation or careless handling. The new design has an orifice diameter of 1/4 inch which should eliminate clogging of the valve. The entire 750 hour system with the mechanical valve and the new pump-out valve is depicted in Fig. 28.

5. PERMANENT MAGNET STUDIES

The modified DE engine reported in the first quarterly was disassembled and examined following the tests reported in EOS Report 4920-Q-1. As anticipated, the copper accelerating electrode had bowed away from the screen electrode. A permanent set of 0.025 inches was measured. The strength of the permanent magnets was unchanged.

5.1 Permanent Magnet Engine Design

A new engine was designed to test the feasibility of replacing the engine shell with a cylindrical permanent magnet. Details of the design can be seen in Fig. 29. The cylinder was rolled from 0.016 inch thick Vicalloy sheet and electron beam welded to two iron rims. The cathode and anode are similar to the DE design. The accelerator support insulators were mounted further from the electrode gap and were attached to the front rim of the shell by flexures which allow free radial displacement. A higher thermal impedance between the shell and the accelerator was used than on the DE design.

The screen electrode and cathode plate were made from pure iron to form the pole pieces of the magnetic circuit. An intermediate hole pattern was used between the central and peripheral patterns. This was done to alleviate the sudden change in ion-optics noticed on the DE engine and reported in the next section of this report.

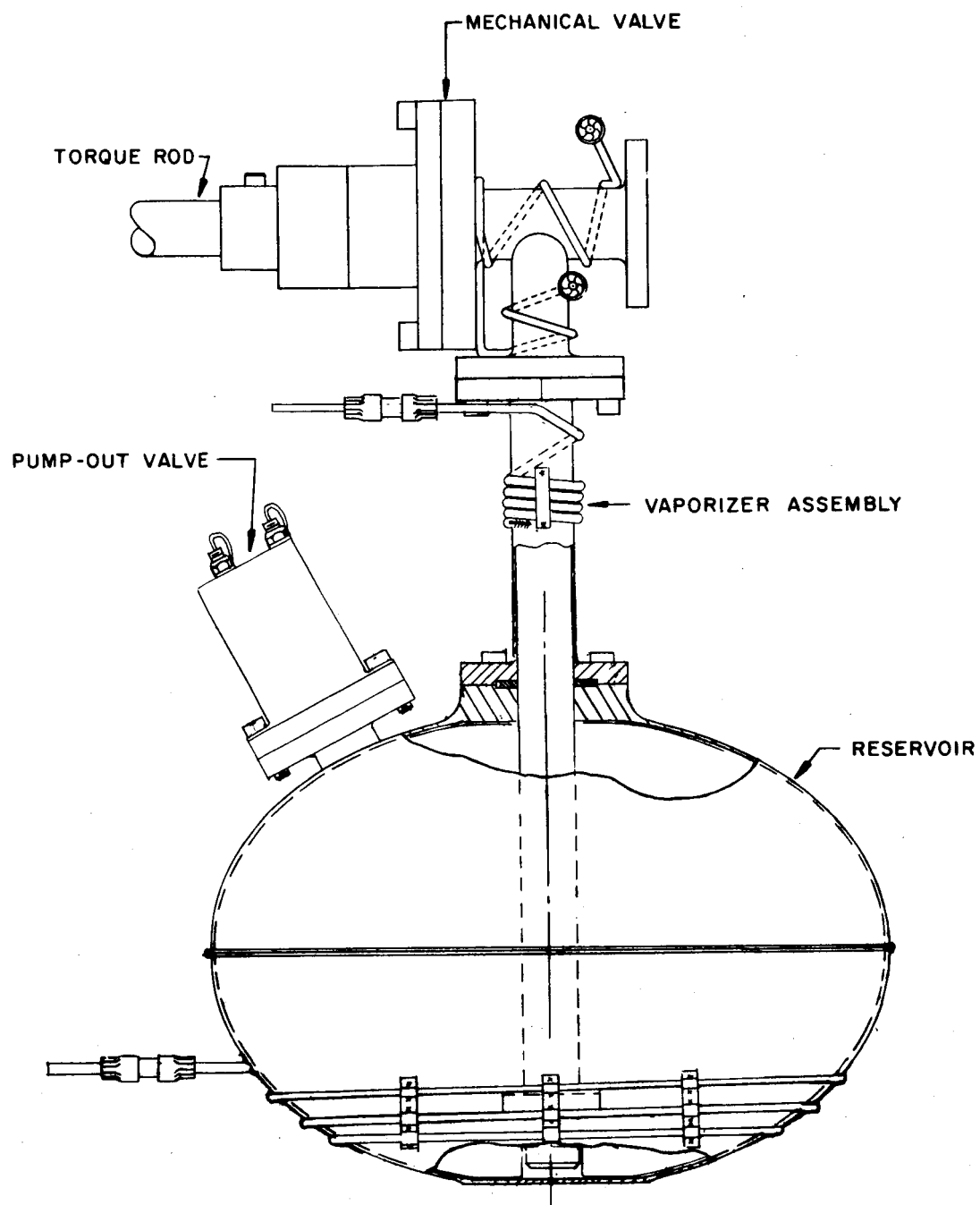


FIG. 28 750-HOUR FEED SYSTEM

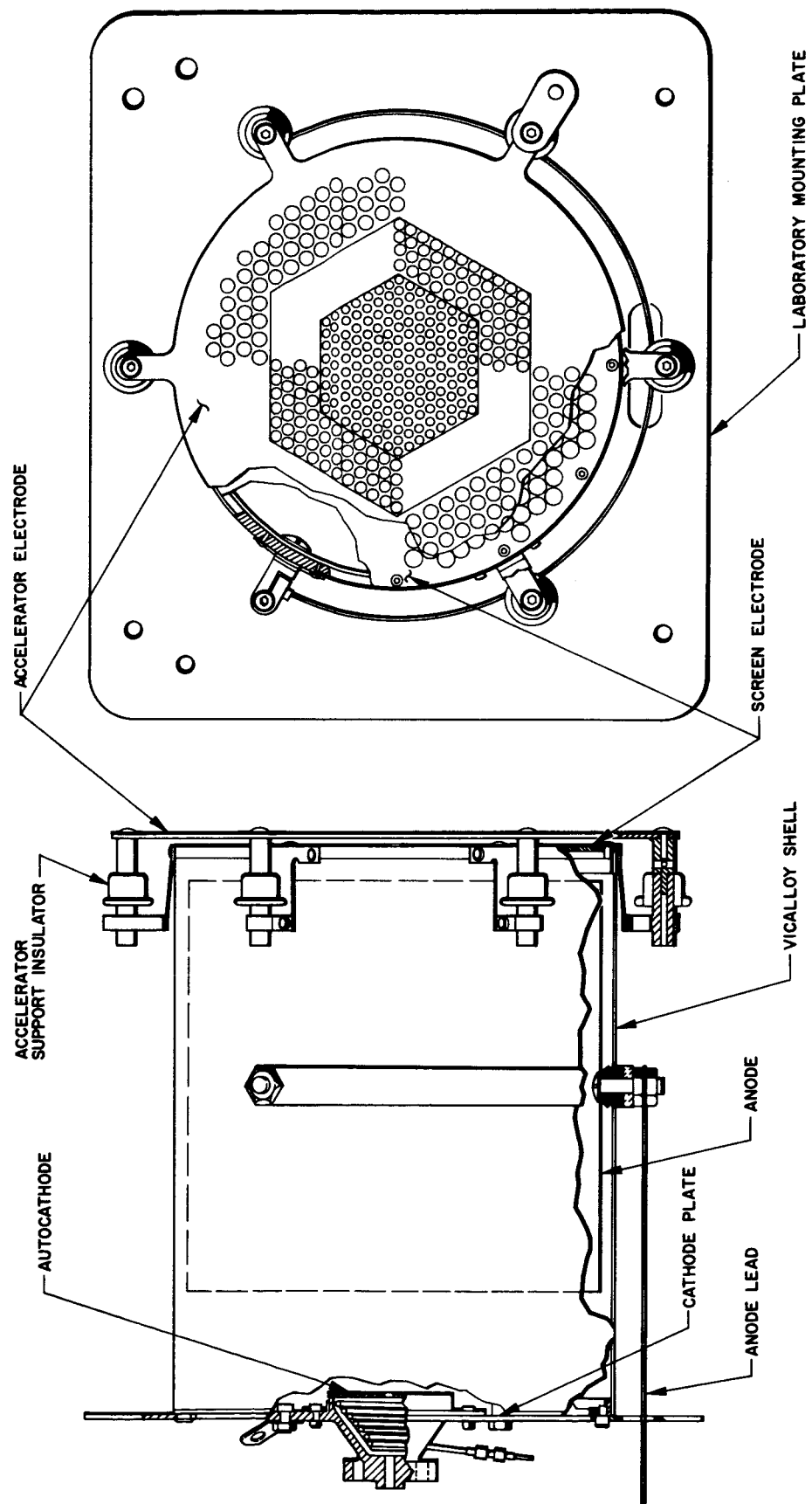


FIG. 29 PERMANENT MAGNET ENGINE DESIGN

5.2 Permanent Magnet Engine Test

The permanent magnet engine was fabricated and tested briefly. The engine is shown in Fig. 30. A copper accelerating electrode was used for the first tests. The cylinder was magnetized fully, producing a field of 22 gauss in the center of the engine, and demagnetized to a field of approximately 8 gauss. The engine operated at a mass efficiency of only 84 percent compared with about 91 percent for the DE engine. (Higher mass efficiencies could be obtained but only at the expense of arc power). The arc current for a given flowrate and arc voltage was about 25 percent higher than experienced with the DE engine. These factors indicate that magnetic field was too low. Further tests, including magnetic field mapping, will be performed in an attempt to improve the performance of this engine.

If the performance of this source can be increased to the level obtained with the DE engine, the weight reduction will be significant. Weights of the DE engine and permanent magnet engine are shown in Table VII. As shown, the principle weight reductions are due to elimination of the magnet coils and a lightening of the anode made possible by rolling the anode from sheet stock rather than machining it from copper pipe.

6. PLASMA DISTRIBUTION STUDIES

6.1 Ion Efflux Distributions

Ion efflux distributions were measured for the permanent magnet modification and electromagnet versions of the DE engine. These are shown in Fig. 31a and 31b respectively. These figures are photographs of oscilloscope traces with the vertical deflection proportional to the probe position. The dip near the edge of the curves is caused partly by the small area free of apertures at the radius where aperture sizes are changed. The main reason, however, for the dip appears to be the change in focussing and collimation of the ion efflux across the aperture size transition region. The dip in the center of the

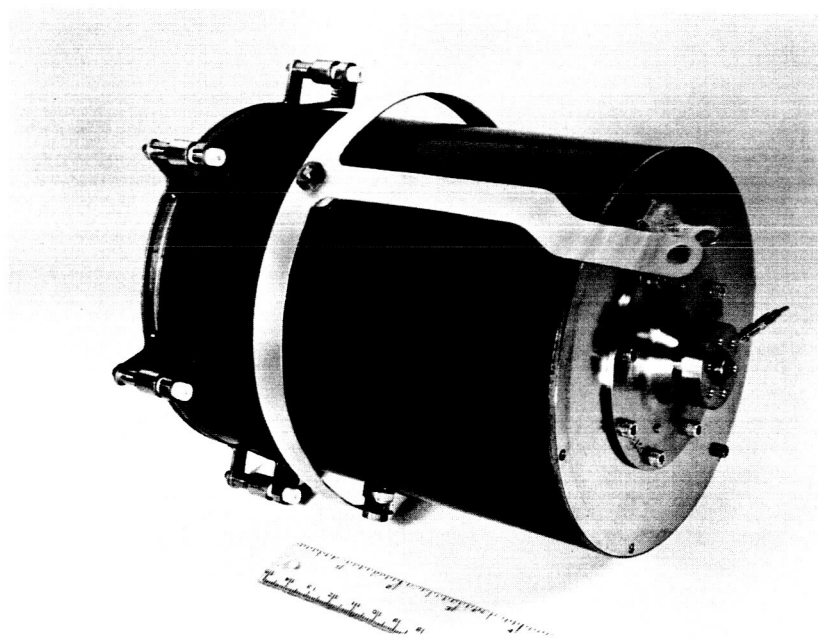
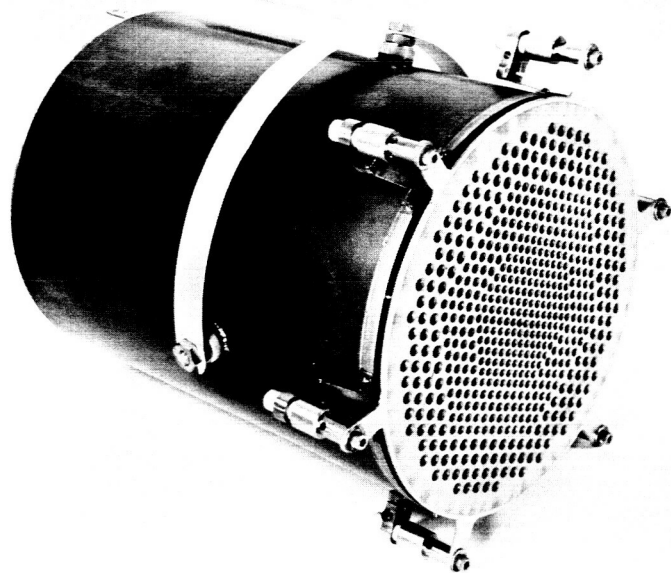
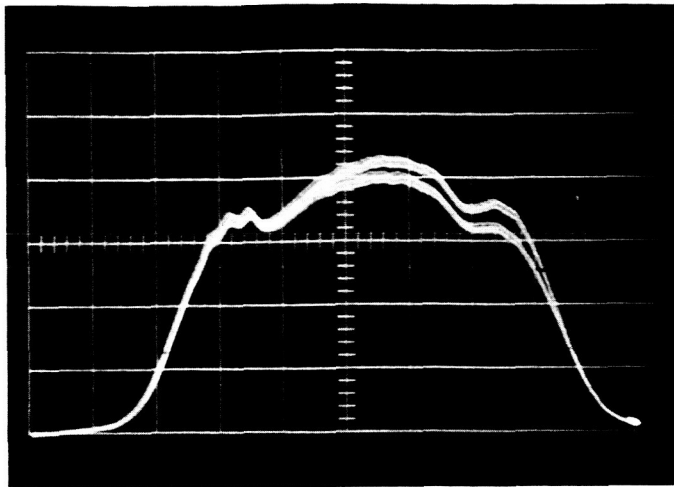


FIG. 30 PERMANENT MAGNET ENGINE

TABLE VII

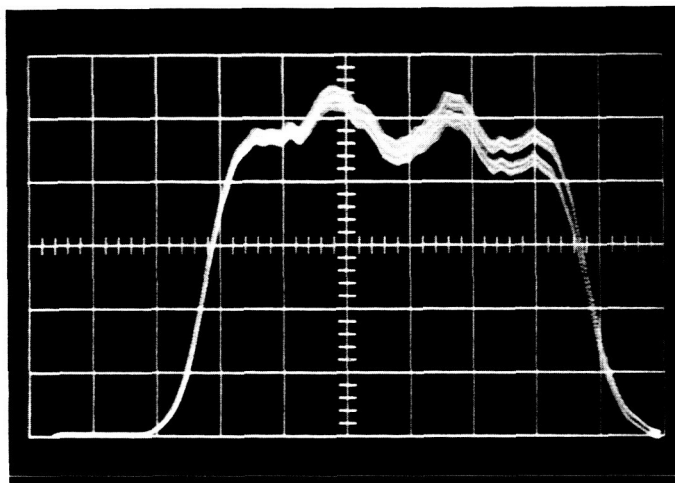
DE and Permanent Magnet Engine Weights

<u>Component</u>	<u>Weight (grams)</u>	
	<u>DE Engine</u>	<u>PM Engine</u>
Shell Assembly	745	364
Anode	360	245
Cathode Assembly	98	98
Cathode Plate	136	57
Screen Electrode	118	38
Accelerator Electrode (Cu)	141	160
Assembled Engine (includes anode and electrode supports)	1956	1112



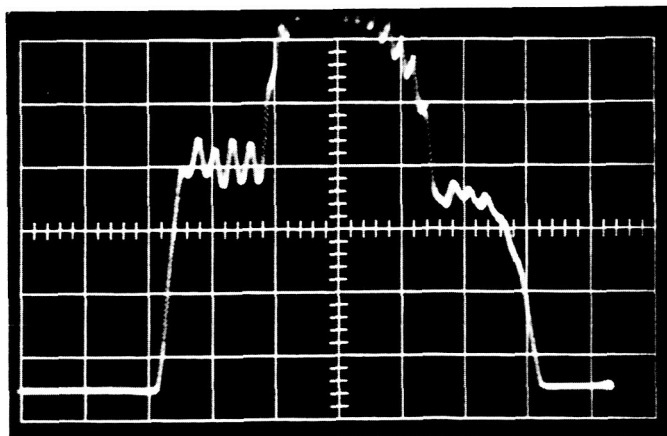
$V_+ = 3.5 \text{ kv}$
 $V_- = -1.0 \text{ kv}$
 $I_B = 400 \text{ ma}$
 $P_A = 292 \text{ watts}$

(a) DE Engine with permanent magnets



$V_+ = 3.8 \text{ kv}$
 $V_- = -1.1 \text{ kv}$
 $I_B = 420 \text{ ma}$
 $P_A = 300 \text{ watts}$
 $I_M = 1.9 \text{ amps}$

(b) DE Engine



$V_+ = 3.0 \text{ kv}$
 $V_- = -1.2 \text{ kv}$
 $I_B = 365 \text{ ma}$
 $P_A = 336 \text{ watts}$
 $I_M = 1.9 \text{ amps}$
 Collimated Probe

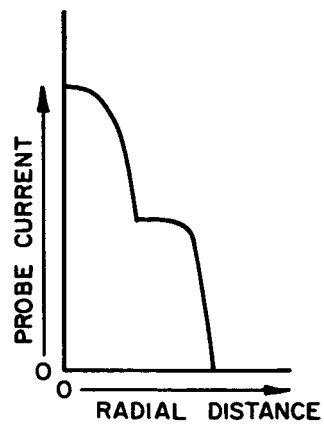
(c) DE Engine

FIG. 31 ION BEAM CURRENT DENSITY DISTRIBUTIONS

distribution of Fig. 31b was due to masking of a radial row of screen electrode apertures to allow thermocouple measurements of accelerator electrode temperatures. With this exception, the two profiles are quite similar.

Figure 31c is an ion efflux distribution measured from the DE engine using a collimated Faraday probe. Collimation was obtained by adding an additional aperture to the probe. This probe measures only those ions which are exhausted along the axis of the probe and has a very small angular acceptance (~ 2 degrees). The integral of the observed distribution over the area of the engine is therefore only a fraction (about 20 percent) of the total ion beam. Information obtained with this probe is strongly dependent upon focussing as can be seen in the curves of Figures 32, 33, and 34. These curves were obtained in the same manner as those of Fig. 31, using the collimated probe. The two sides of the curves were averaged to eliminate a slight skew which was present due to probe misalignment.

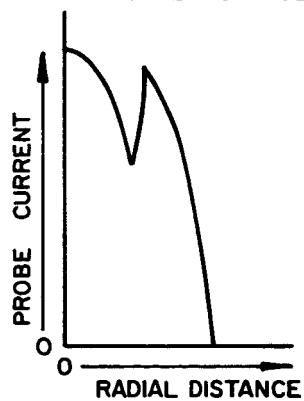
Figures 32 and 33 show the effect of variations in source potential and accelerator electrode potential respectively. From the three curves of Fig. 32 it appears that the higher the source potential the better the focussing. High source potential, however, tends to make the change in ion optics more drastic across the transition between the two hole patterns used. Figure 33 indicates that the closer the accelerator electrode potential is to ground potential, the better the focussing. This is expected since the decelerating region downstream from the accelerator electrode slows the exhausted ions in the axial direction but does not greatly affect transverse velocities. Thus, for a given trajectory to the accelerator (constant current and accelerating gap potential) higher decelerating potential drops will increase the angle between the exhausted ion and the engine axis. This probe may allow more thorough evaluation of the ion optics of various electrode systems than was previously possible for the gas discharge engines.



$V_+ = 3.0 \text{ kv}$
 $V_- = -1.2 \text{ kv}$
 $P_A = 336 \text{ watts}$
 $I_B = 365 \text{ ma}$
 $I_M = 1.9 \text{ amps}$
 (a)

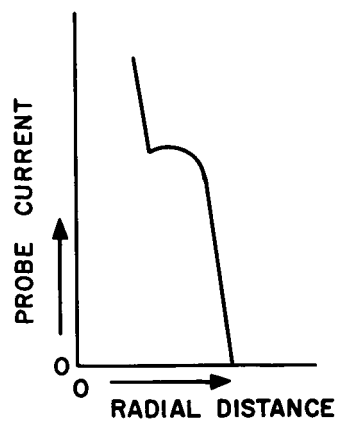


$V_+ = 3.5 \text{ kv}$
 $V_- = -1.2 \text{ kv}$
 $P_A = 336 \text{ watts}$
 $I_B = 375 \text{ ma}$
 $I_M = 1.9 \text{ amps}$
 (b)

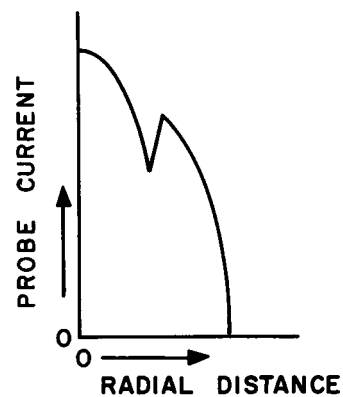


$V_+ = 4.0 \text{ kv}$
 $V_- = -1.2 \text{ kv}$
 $P_A = 328 \text{ watts}$
 $I_B = 370 \text{ ma}$
 $I_M = 1.9 \text{ amps}$
 (c)

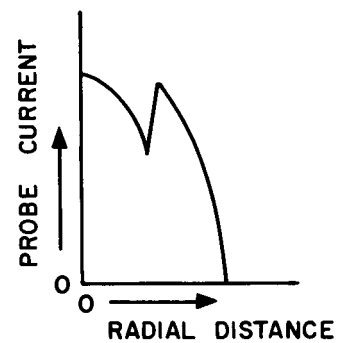
FIG. 32 VARIATION OF ION CURRENT DENSITY DISTRIBUTION WITH SOURCE POTENTIAL



$V_+ = 3.5 \text{ kv}$
 $V_- = -0.9 \text{ kv}$
 $P_A = 328 \text{ watts}$
 $I_B = 370 \text{ ma}$
 $I_M = 1.9 \text{ amps}$
 (a)



$V_+ = 3.5 \text{ kv}$
 $V_- = -1.2 \text{ kv}$
 $P_A = 336 \text{ watts}$
 $I_B = 375 \text{ ma}$
 $I_M = 1.9 \text{ amps}$
 (b)



$V_+ = 3.5 \text{ kv}$
 $V_- = -1.5 \text{ kv}$
 $P_A = 328 \text{ watts}$
 $I_B = 370 \text{ ma}$
 $I_M = 1.9 \text{ amps}$
 (c)

FIG. 33 VARIATION OF ION CURRENT DENSITY
 DISTRIBUTION WITH ACCELERATOR
 POTENTIAL

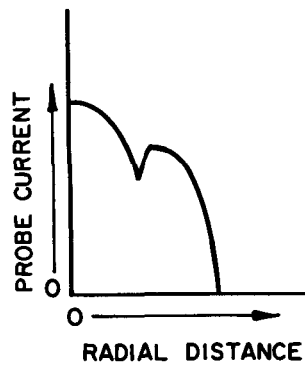
Figure 34 shows ion efflux profiles obtained with different values of magnetic field. As previously reported, the higher magnetic fields cause the distribution to peak at the center.

6.2 LN₂ Cooled Neutral Detector

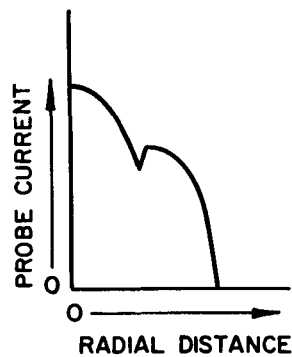
A schematic of the new neutral detector which was built to operate in the ion beam is shown in Fig. 35. Ions entering the front aperture see a transverse electric field which deflects them up through the grid and out of the detector. Two apertures are used after the sweep electrodes so that re-evaporated cesium from the sweep area will not be measured. The entire detector is liquid nitrogen cooled to capture stray cesium atoms on the walls of the device thus preventing a cesium pressure build-up. Neutral cesium atoms arriving at the filament are ionized by contact ionization and repelled from the filament which is biased positive with respect to the detector walls. A portion of these ions are intercepted by the collector and measured. The detector will be mounted on the probe drive used for the tests described above so that neutral efflux measurements as a function of radial position can be obtained. This probe has been fabricated and will be operated during the next quarter. The collimated Faraday probe described above will also be mounted with the cooled neutral detector to allow simultaneous scanning of both ion and neutral efflux distributions.

7. AUTOCATHODE IMPROVEMENT STUDIES

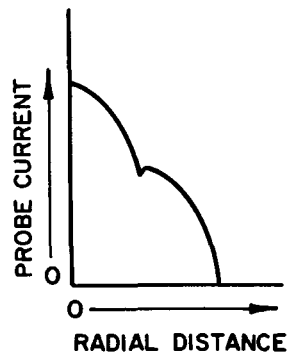
The externally heated autocathode reported in the first quarterly report was modified and tested further. The emitter in the first design was mounted between the cathode housing and the orifice plate. During preheating the orifice plate acted as a heat sink which caused the emitter temperature to run cooler than the housing. In order to increase the emitter temperature during preheating, a corrugated cylinder of tantalum was inserted between the emitter and the housing.



$V_+ = 3.5 \text{ kv}$
 $V_- = -1.2 \text{ kv}$
 $P_A = 364 \text{ watts}$
 $I_B = 380 \text{ ma}$
 $I_M = 1.7 \text{ amps}$
 (a)



$V_+ = 3.5 \text{ kv}$
 $V_- = -1.2 \text{ kv}$
 $P_A = 372 \text{ watts}$
 $I_B = 380 \text{ ma}$
 $I_M = 1.9 \text{ amps}$
 (b)



$V_+ = 3.5 \text{ kv}$
 $V_- = -1.2 \text{ kv}$
 $P_A = 366 \text{ watts}$
 $I_B = 380 \text{ ma}$
 $I_M = 2.1 \text{ amps}$
 (c)

FIG. 34 VARIATION OF ION CURRENT DENSITY DISTRIBUTION WITH MAGNETIC FIELD

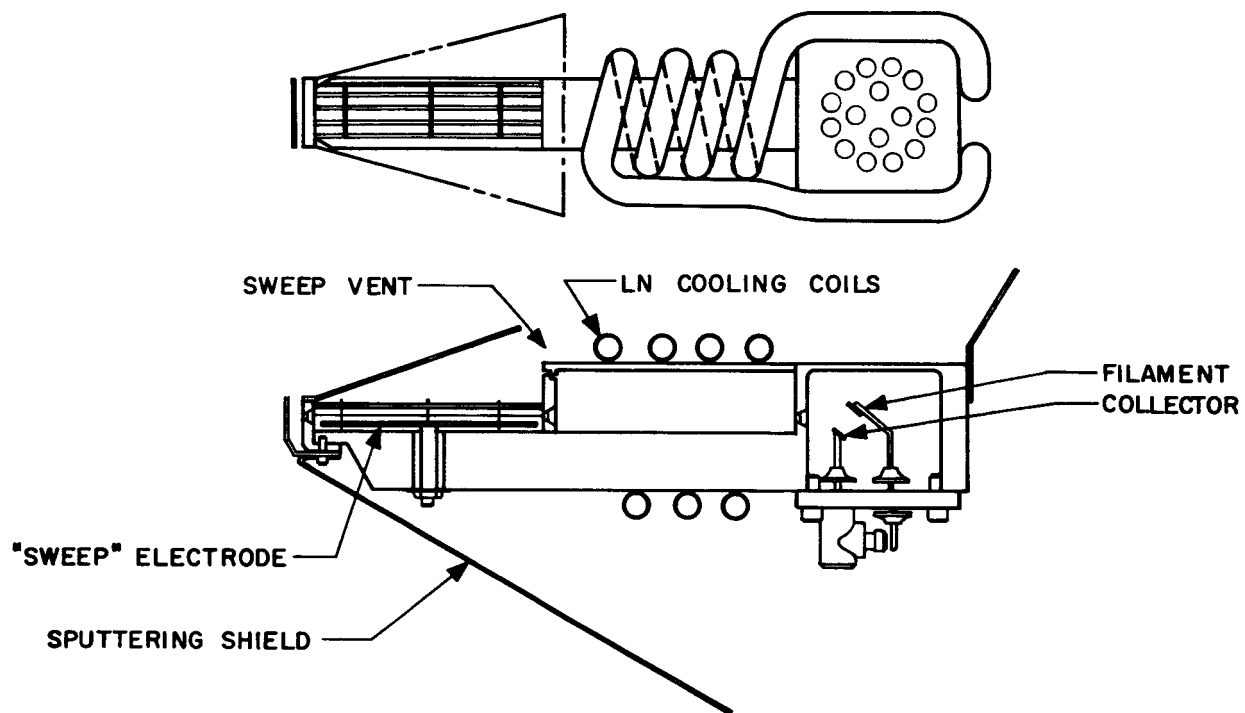


FIG. 35 LIQUID NITROGEN COOLED, SCANNING NEUTRAL DETECTOR

Subsequent Starts with 52 watts of heater power and a housing temperature of 410°C were successful. The housing ran hotter during autocathode operation, however, and the source efficiency was reduced.

7.1 Autocathode Tests

A series of emitter structures, supported only by the housing walls, were fabricated. These emitters were spirals of tantalum strip fastened to the housing at both ends. The cross section and number of turns were varied to obtain different thermal and electrical impedances from the emitter to the housing. Four of these emitters were tested in a DE engine. The main difference in operating parameters which could be observed was a difference in overall source efficiency as shown by the data in Table VIII. As shown, the second and third emitters were superior. These two cathodes also started more smoothly.

7.2 Cathode Starting Power

To determine the feasibility of eliminating the separate cathode heater power supply, the heater on the externally heated cathode was connected to the arc power supply. A relay operated by the normal cathode heater interlock was used to disconnect the heater when the arc current exceeded 20 amperes. The impedance of the heater which was only 2 ohms, limited the maximum voltage to about 14 volts (100 watts). With this low voltage the arc was more difficult to start. The cathode heater was turned off during one test when an arc of about one ampere was established. This reduced the load on the arc power supply causing the voltage to rise. This procedure allowed a smooth start. By changing the turn-off level in this manner or by further increasing the cathode heater impedance, the cathode heater supply requirement can easily be reduced to the function of a switch. No overload of the arc power supply would occur since the cathode heater is used only when the arc current is well below its capacity.

TABLE VIII
Source Efficiency with External
Heater Cathodes

<u>Emitter No.</u>	<u>1</u>	<u>2</u>	<u>3</u>	<u>4</u>
Thickness (inches)	0.010	0.010	0.010	0.005
Width (inches)	0.5	0.25	0.125	0.125
No. of turns	1	2	4	4
Flowrate (amp)	0.452	0.425	0.435	0.430
Mass Efficiency (%)	81.5	89	87.4	84.5
Source Energy per Beam Ion (kev/ion)	0.658	0.675	0.624	0.989

8. QUALITY ASSURANCE

Shop traveller activity during the second quarter continued to provide DER engine and zero-gravity feed system support. Equipment logs were issued for DER-2 engine and a second zero-gravity feed system. Four standing assembly requests are active; one each for DER-1 engine, DER-2 engine, 4923 S/N 1 zero-gravity feed system and 4923 S/N 2 zero-gravity feed system.

Ion Physics Electrical Laboratory Calibration Procedure revision C.P. 3670A was released. This revision reflects the fact that the EOS Standards Laboratory maintains records showing that calibrations are traceable to the National Bureau of Standards. In addition, calibration data and deterioration trend data are being maintained in one laboratory log book rather than two.

Special processing instructions were issued for vacuum brazing of tantalum to molybdenum with palladium-cobalt filler material.

Failure reporting to date is summarized in the following tabulation:

Total number of failures reported	7
Corrective action taken	3
Corrective action not required	4
Outstanding	0

9. PLANS FOR NEXT QUARTER

During the next quarter, DE engine tests will be pursued to determine the suitability of various electrode materials with respect to the high drain condition. A new engine will be designed and prepared for a 750 hour test. The accelerating electrode for this engine will be chosen on the basis of the results of the electrode material tests.

The permanent magnet engine will be tested with shell magnets of various field strengths. The performance of the permanent magnet engine will be evaluated over a wide range of operating conditions.

Plasma distribution studies will be pursued for various engine configurations using the new neutral cesium detector and Faraday probe. Investigations of autocathode configurations will continue with emphasis on achieving high source efficiencies.